

---

# Optimizing the Communication–Accuracy Trade-off in Federated Learning with Rate–Distortion Theory

---

Nicole Mitchell<sup>1</sup> Johannes Ballé<sup>1</sup> Zachary Charles<sup>1</sup> Jakub Konečný<sup>1</sup>

## Abstract

A significant bottleneck in federated learning is the network communication cost of sending model updates from client devices to the central server. We propose a method to reduce this cost. Our method encodes quantized updates with an appropriate universal code, taking into account their empirical distribution. Because quantization introduces error, we select quantization levels by optimizing for the desired trade-off in average total bitrate and update distortion. We demonstrate empirically that in spite of the non-i.i.d. nature of federated learning, the rate–distortion frontier is consistent across datasets, optimizers, clients and training rounds, and within each setting, distortion reliably predicts model performance. This allows for a remarkably simple compression scheme that is near-optimal in many use cases, and outperforms TOP-K, DRIVE, 3LC and QSGD on the Stack Overflow next-word prediction benchmark.

## 1. Introduction

Federated learning (FL) is a machine learning framework in which clients collaboratively train a model under the coordination of a central server or service provider, without sharing their local data. Prototypical FL algorithms such as FedAvg (McMahan et al., 2017) typically involve multiple communication rounds in which clients train on their own local data, sharing only their model updates with the server. While federated learning can incur the benefits of centralized learning without the need to store sensitive user data, it also introduces challenges related to data heterogeneity and network constraints (Kairouz et al., 2021).

Kairouz et al. (2021, Table 1) propose a taxonomy that divides FL into *cross-device* and *cross-silo* regimes, characterized by their practical constraints. In cross-silo FL, there are a small number of computationally reliable clients. In

cross-device FL, there are many intermittently available and computationally unreliable clients. While both regimes face optimization challenges stemming from data heterogeneity and communication constraints (Bonawitz et al., 2019; Ludwig et al., 2020; Liu et al., 2021; Huba et al., 2021; Wang et al., 2021), communication-efficiency is particularly critical in cross-device settings, due to network and bandwidth limitations (Bonawitz et al., 2019).

Cross-device FL also faces challenges due to partial participation. Typically, only a small subset of clients participate in each communication round. Often, each client may only participate once (if at all) throughout the entire training procedure (Kairouz et al., 2021). Thus, in cross-device FL, each communication round often involves a set of clients who have not previously participated, and therefore have no useful *state* learned across previous rounds. Even if we can identify clients who have participated before, such state can suffer from staleness and actually reduce accuracy (Reddi et al., 2021). Thus, cross-device FL typically employs *stateless* algorithms, in which all training quantities used by a client (save for their data) must be provided by the server at each round (e.g., model weights, hyperparameters, etc.).

In this work we focus on compression methods for client updates in cross-device settings. While client updates in algorithms such as FedAvg are not actually gradients (Reddi et al., 2021), client update compression is closely related to gradient compression methods for distributed training. Such methods often employ techniques like quantization (Alistarh et al., 2017; Suresh et al., 2017), sparsification (Aji & Heafield, 2017; Lin et al., 2018), and low rank decomposition (Wang et al., 2018; Vogels et al., 2019) in order to obtain efficiently communicable estimates of gradients.

Although such methods have already been applied to and refined in the context of FL (Sattler et al., 2019; Rothchild et al., 2020; Reiszadeh et al., 2020; Haddadpour et al., 2021), we find that such methods can suffer from a lack of practicality, effectiveness, or flexibility. To that end, we identify three desirable properties of a compression method for FL that (to the best of our knowledge) have not been addressed simultaneously.

---

<sup>1</sup>Google Research. Correspondence to: Nicole Mitchell <nicolemitchell@google.com>.

**Desiderata.** First, we would like our method to be stateless. Many prior compression methods for FL (e.g., Sattler et al. (2019); Rothchild et al. (2020)) cannot be directly applied to the cross-device setting, as they involve stateful compression algorithms. One commonly used stateful component of such algorithms is an error-feedback mechanism, in which the compression error for a given round is maintained and incorporated into the compression of the subsequent round (see (Xu et al., 2020) for a more complete discussion on this). As discussed above, the low participation rate and large number of clients restrict us (practically speaking) to stateless compression methods.

Second, while a number of gradient compression techniques can be applied in a stateless manner, their analysis and effectiveness is often based on their worst-case guarantees (Alistarh et al., 2017; Suresh et al., 2017; Beznosikov et al., 2020; Albasyoni et al., 2020; Vargaftik et al., 2021). While useful in the abstract, this analysis ignores statistical properties of the information to be compressed. By contrast, we observe (and show below) that client updates in FL often have a consistent structure that can be exploited to improve efficiency. Across clients, training rounds, models and optimizers, client updates are often highly sparse and follow a pattern similar to a power law distribution tightly centered around zero. By selecting our compression operator carefully, we can leverage this structure to generate a more efficient representation of a client’s update.

Last, we would like to be able to leverage rate–distortion optimization to guide the design and usage of our method. Notably, lossy compression techniques such as quantization introduce error and yield a trade-off between the size of the compressed quantity (*bitrate*  $R$ ) and its fidelity (*distortion*  $D$ ). Different applications of FL may target a specific rate or a specific distortion, while minimizing the other, or may aim to minimize both jointly. By basing our choice of updates on rate–distortion optimization, we develop a method that allows us to trade off between model performance and communication cost.

**Contributions.** In this work, we develop a method that combines the three desirable characteristics above. Specifically, our contributions are summarized as follows:

- We propose a novel compression method applicable in cross-device FL settings, which yields better rate–distortion trade-offs, as well as better accuracy at the same bitrate, compared to existing methods.
- We ground our method in empirical characteristics of model updates communicated in FL, and use a universal code with cost only slightly exceeding the entropy of the signal.
- We parameterize our method in such a way that allows us to optimize for the global rate–distortion frontier and select the necessary trade-off on each client, while avoiding direct optimization at the client.
- We show that popular preprocessing by a random rotation can hurt average-case performance, as it hides the statistical regularities that could be exploited for compression, and *increases* the entropy of the signal to be communicated.
- We show that normalizing each client’s update, a technique common in compression methods for decentralized learning, is sub-optimal in non-i.i.d. FL settings.
- Our method outperforms TOP-K, DRIVE, 3LC and QSGD on the Stack Overflow next-word prediction task, raising the accuracy–communication cost frontier.

## 2. Method

In FL, we often wish to find a model  $\theta \in \mathbb{R}^d$  that minimizes a weighted average of client loss functions

$$\min_{\theta} f(\theta) := \sum_{k=1}^K w_k f_k(\theta) \quad (1)$$

where  $K$  is the total number of clients and  $f_k, w_k$  are the loss function and weight of client  $k$ . For practical reasons,  $w_k$  is often the number of examples held by client  $k$  (*example weighting*), which can incur optimization benefits (Li et al., 2020). We wish to solve (1) without sharing data and with minimal client-to-server communication. To do so we combine FedOpt (Reddi et al., 2021) (generalizing FedAvg (McMahan et al., 2017)) with compression.

In the FedOpt framework, at each round  $t$ , the server broadcasts its model  $\theta_t$  to a set of clients  $\mathcal{S}_t$ . Each client  $k \in \mathcal{S}_t$  uses a procedure LOCALTRAIN to train its model locally. LOCALTRAIN( $\theta, f$ ) is often multiple steps of SGD on  $f$  starting at  $\theta$ . After computing  $\theta_t^k = \text{LOCALTRAIN}(\theta_t, f_k)$ , the client sends its weighted update  $u_t^k := w_k(\theta_t^k - \theta_t)$  to the server.

---

### Algorithm 1 FedOpt with compression

---

**Input:** Number of rounds  $T$ , initial model  $\theta_0 \in \mathbb{R}^d$ , LOCALTRAIN, SERVERUPDATE, encoder  $\mathcal{E}$ , decoder  $\mathcal{D}$

**for**  $t = 0, \dots, T$  **do**

$\mathcal{S}_t \leftarrow$  (random set of  $m$  clients)

Broadcast  $\theta_t$  to all clients  $k \in \mathcal{S}_t$

**for** each client  $k \in \mathcal{S}_t$  **in parallel do**

$\theta_t^k \leftarrow \text{LOCALTRAIN}(\theta_t, f_k)$

Compute  $u_t^k = w_k(\theta_t^k - \theta_t)$

Send  $c_t^k = \mathcal{E}(u_t^k)$  to the server

**end for**

$g_t \leftarrow \frac{\sum_{k \in \mathcal{S}_t} \mathcal{D}(u_t^k)}{\sum_{k \in \mathcal{S}_t} w_k}$

$\theta_{t+1} \leftarrow \text{SERVERUPDATE}(\theta_t, g_t)$

**end for**

---

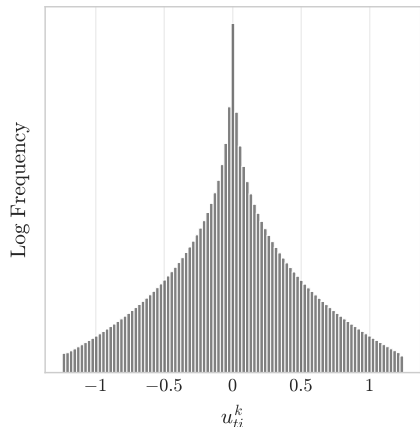


Figure 1. Histogram of coordinate values of weighted client updates, averaged over the course of training across all participating clients in Stack Overflow NWP.

To reduce communication, clients can instead send a compressed update  $c_t^k := \mathcal{E}(u_t^k)$  to the server, where  $\mathcal{E}$  is some encoder. The server decodes the client updates using a decoder  $\mathcal{D}$ , and computes a weighted average  $g_t$  of the  $\mathcal{D}(c_t^k)$  (using the weight  $w_k$ ). Finally, the server updates its model using a procedure `SERVERUPDATE`. As proposed by Reddi et al. (2021), `SERVERUPDATE` is typically a first-order optimization step, treating  $g_t$  as a gradient estimate, with server learning rate  $\eta_s$ . For example, if `SERVERUPDATE` is gradient descent, then  $\text{SERVERUPDATE}(\theta, g) = \theta - \eta_s g$ .

Algorithm 1 summarizes our framework. Similar algorithms appear elsewhere (e.g., Haddadpour et al., 2021). The focal point of our work is in developing appropriate encoding and decoding operators  $\mathcal{E}, \mathcal{D}$  based on rate-distortion theory that satisfy the desiderata above. In the remainder of this section, we lay out the observations and derivations that underpin our choices.

## 2.1. Quantization

In order to efficiently communicate client updates, we reduce their fidelity via quantization (Gray & Neuhoff, 1998). We focus on coordinate-wise (scalar) quantization due to its computational tractability. In order to choose an appropriate quantization method, we track the statistical structure of client updates over the course of training using FedOpt on various FL tasks (see Section 3). We find that across tasks, optimizers, model layer types, clients and training rounds, the weighted client updates follow a consistent symmetric, unimodal, sparse, and heavy-tailed distribution centered around zero, as illustrated in Figure 1.<sup>1</sup>

Given this statistical structure, there are two efficient ways

<sup>1</sup>Throughout the main body of the paper, we present results on the Stack Overflow NWP task (details in Appendix A), with full results on other tasks presented in Appendix B.

to represent this data: using a fixed-length bit representation of each possible quantized value (Konečný et al., 2016; Vargaftik et al., 2021), or using a variable-length bit representation (Suresh et al., 2017; Alistarh et al., 2017) to represent more likely values with shorter bit sequences, optimizing average representation length (see Section 2.2). In addition, we can decide to limit quantization to uniform quantization (i.e., rounding), where the size of each quantization bucket is identical, which has computational benefits.

While using a fixed-bit representation has advantages in differential privacy applications, when combined with uniform quantization such an approach would be inefficient in our setting, effectively representing extremely likely and extremely unlikely values with the same number of bits. Ideally, one would adjust the quantization boundaries such that each quantization bucket has approximately equal likelihood. However, nonuniform quantization would generally produce biased decoded client updates (i.e.,  $\mathbb{E}[\mathcal{D}(\mathcal{E}(u_t^k))] \neq u_t^k$ ), and is computationally more complex than rounding.

Thus, we elect to use variable-length representations with uniform quantization. We quantize client updates by scaling by a positive quantization step size  $\Delta \in \mathbb{R}_{>0}$ , and rounding coordinate-wise using one of three methods: `DETERMINISTICROUND`, `STOCHASTICROUND`, and `DITHEREDROUND`. The quantization step size  $\Delta$  controls the granularity with which continuous client update values are discretized: a large  $\Delta$  yields low-resolution client updates with smaller information content, while a small  $\Delta$  yields high-resolution client updates with more information to be transmitted.

`DETERMINISTICROUND`( $u, \Delta$ ) rounds  $u/\Delta$  to the nearest integer. For  $q = \text{STOCHASTICROUND}(u, \Delta)$ ,

$$q = \begin{cases} \lceil u/\Delta \rceil, & \text{with prob. } p = u/\Delta - \lfloor u/\Delta \rfloor \\ \lfloor u/\Delta \rfloor, & \text{with prob. } 1 - p. \end{cases}$$

`DITHEREDROUND`( $u, \Delta$ ) samples  $z \sim \mathcal{U}(-.5, .5)$  and rounds  $u/\Delta + z$  to the nearest integer, subtracting  $z$  again on the decoder (Schuchman, 1964). In practice,  $z$  is generated pseudo-randomly from a seed so that it is available on both sides. Note that the latter two methods give unbiased estimates of  $u/\Delta$ .

**Empirical Evaluation.** We find that for a full range of quantization step sizes  $\Delta$ , `STOCHASTICROUND` consistently outperforms `DETERMINISTICROUND` and `DITHEREDROUND` across datasets, tasks and optimizers. `DITHEREDROUND` is found to be unsuitable for our FL simulations, as the added noise requires lower learning rates at coarser quantization levels which slows convergence. Across quantization step sizes  $\Delta$ , there is much less variance in the accuracy over training when using `STOCHASTICROUND`, as depicted in Figure 2. In the sequel, we only use `STOCHASTICROUND`.

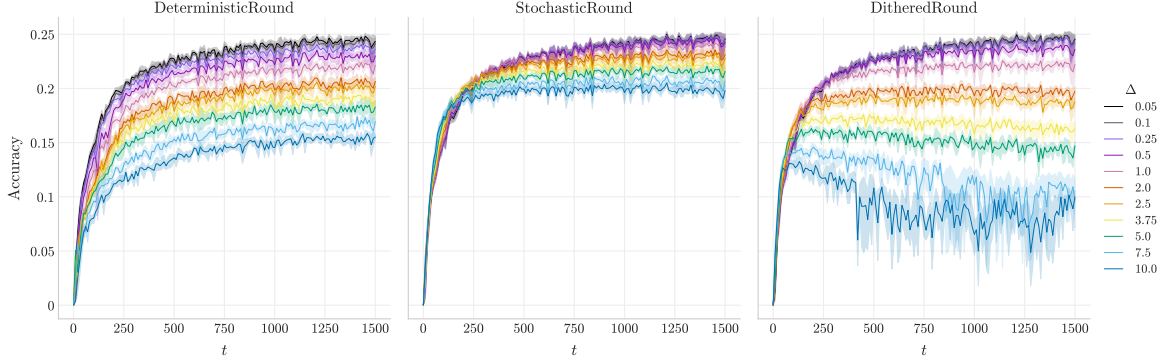


Figure 2. Accuracy versus round  $t$  for varying quantization step sizes and rounding methods on Stack Overflow NWP.

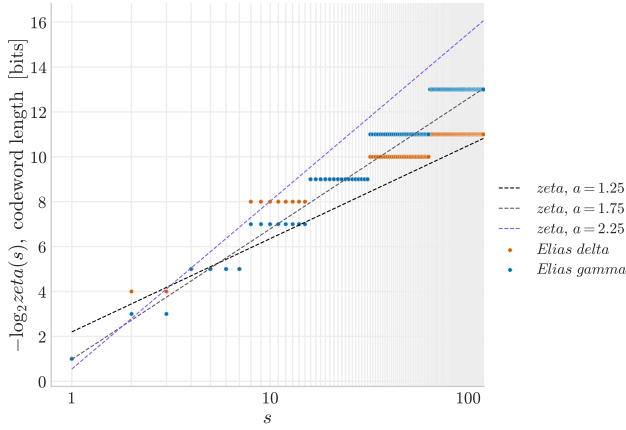


Figure 3. *Elias gamma* and *Elias delta* codeword lengths for the integers roughly follow a *zeta* distribution.

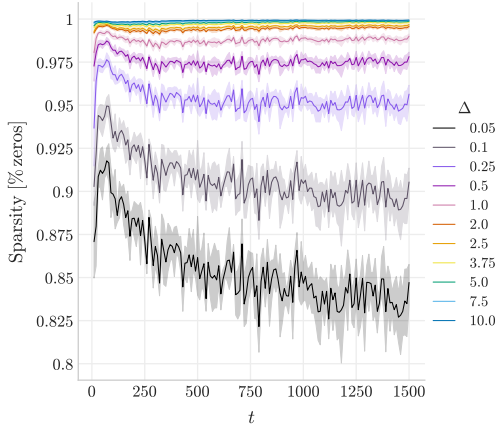


Figure 4. Average sparsity of quantized client updates across step sizes in Stack Overflow NWP.

## 2.2. Entropy Coding

With client updates  $u_t^k$  quantized to integer values  $q_t^k$ , we apply two *entropy coding* techniques that exploit statistical structure to yield smaller representations without extra distortion: *universal coding* and *run length encoding*. As

variable-length codes, entropy codes map symbols of the source alphabet, in this case the integers, to binary codewords:  $\mathbb{Z} \rightarrow \{0, 1\}^*$ . According to Shannon’s source coding theorem, the least possible average number of bits required to communicate a discrete sequence is the entropy of that sequence (Shannon, 1948). Entropy codes aim to represent a symbol  $s$  with a codeword (bit sequence) close in length to  $-\log_2 \text{Prob}(s)$ , such that in expectation, the bitrate is close to the sequence’s entropy.

**Universal Coding.** Since the empirical distribution of client updates closely resembles a symmetric, double-sided power law (with a spike at zero, see Figure 1), we consider using the *gamma* and *delta* universal codes (Elias, 1975) to encode the magnitude of each non-zero quantized coordinate of  $q_t^k$ . As depicted in Figure 3, both of these codes reasonably match a *zeta distribution*, the discrete version of a power law, making them good candidates.

Additionally, these codes admit worst-case guarantees, i.e. the expected bitrates of the *gamma* and *delta* codes are upper bounded by  $3\times$  and  $4\times$  the entropy of the empirical distribution, respectively, as long as probability decreases with magnitude (Elias, 1975). They also do not require bounding the integer magnitudes from above as other codes would, which eliminates a hyperparameter. The signs of the non-zero coordinates can be encoded efficiently using one additional bit per non-zero coordinate, since the empirical distribution is very close to symmetric.

**Run Length Encoding.** The likelihood of zero coordinates is significantly higher than suggested by a power law, i.e., client updates are sparse in an  $\ell_0$  sense, as illustrated in Figure 4. To efficiently communicate these sparse tensors, we encode the number of repeated zeros between each non-zero coordinate, rather than transmitting each occurrence. For simplicity of implementation, we reuse the same universal code that we use for the non-zero magnitudes.

**Empirical Evaluation.** We measure how the average codeword lengths using the *delta* and *gamma* codes compare to the entropy of the client updates and observe which of

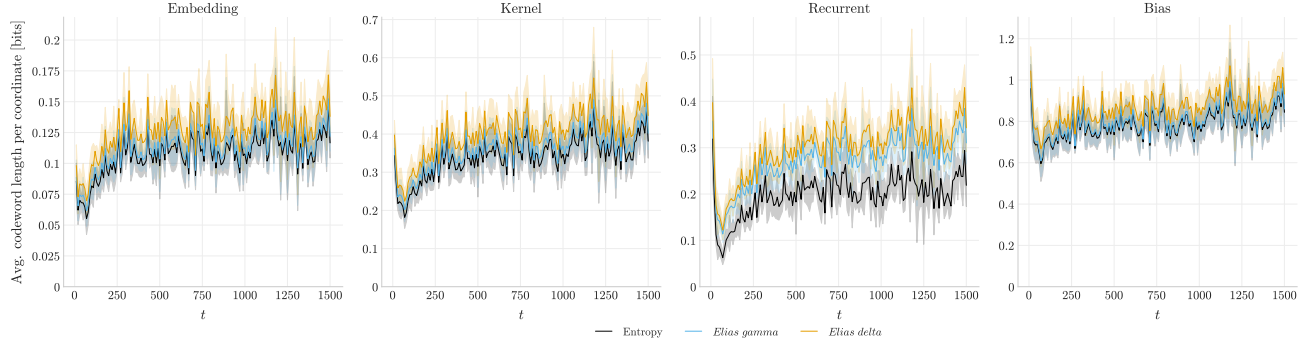


Figure 5. Average codeword length of Elias gamma and delta codes when applied to quantized client updates in Stack Overflow NWP with  $\Delta = 0.05$ , as well as the entropy. Results are plotted for each layer type of the model.

---

**Algorithm 2** Client-side encoder  $\mathcal{E}$ 


---

**Input:** client update  $u \in \mathbb{R}^d$ , quantization step size  $\Delta > 0$   
**Output:** encoded client update  $c \in \{0, 1\}^*$   
 $q \leftarrow \text{STOCHASTICROUND}(u, \Delta)$   
 $c \leftarrow \square; i \leftarrow 0$   
**while**  $i < d$  **do**  
 $r \leftarrow \text{LEADINGZEROS}(q_i)$   
 $c \leftarrow c \oplus \text{GAMMA}(r + 1); i \leftarrow i + r$   
 $c \leftarrow c \oplus \text{SIGN}(q_i) \oplus \text{GAMMA}(|q_i|); i \leftarrow i + 1$   
**end while**  
**return**  $c$

---

these universal codes has the smaller rate (Figure 5). We test this across training rounds, quantization step sizes, datasets, tasks, and model layer types. We find that the *gamma* code consistently outperforms the *delta* code with an acceptable overhead over the entropy of the client updates, typically less than 20%, independently of how finely we quantize.

The observations above lead us to the encoding operator  $\mathcal{E}$  given in Algorithm 2. We let  $\square$  denote the empty binary string and  $\oplus$  denote concatenation of binary strings, e.g.  $110 \oplus 10 = 11010$ . The decoding operator  $\mathcal{D}$  simply consists of parsing the *gamma* code from the binary string, inserting zeros, recovering signs, and multiplying by  $\Delta$ .<sup>2</sup>

### 2.3. Rate–Distortion Optimization

With the encoder algorithm determined, we aim to achieve the desired trade-off between total bitrate and final model performance by controlling the quantization parameters. For example, we may wish to optimize the performance of the model (e.g., final accuracy), given that the total rate  $R$  stay below an acceptable bitrate budget  $B$ :

$$\min f(\theta) \text{ s.t. } R(\mathcal{Q}) = \sum_{t,k} |\mathcal{E}(u_t^k, \Delta_t^k)| \leq B, \quad (2)$$

<sup>2</sup>Encode and decode ops available in TensorFlow Compression: <https://github.com/tensorflow/compression>

where  $\Delta_t^k$  is the quantization step size used by client  $k$  in round  $t$ , chosen by a policy  $\mathcal{Q}$ .

To avoid additional server–client communication or state, we need an adequate proxy for final model performance that is tractable to predict from data available at the client. For this, we consider total distortion

$$D(\mathcal{Q}) = \sum_{t,k} \|u_t^k - \mathcal{D}(\mathcal{E}(u_t^k, \Delta_t^k), \Delta_t^k)\|_2^2, \quad (3)$$

yielding the *rate–distortion optimization* problem  $\min D(\mathcal{Q})$  s.t.  $R(\mathcal{Q}) \leq B$  (Cover & Thomas, 2006, Chapter 10). We verify empirically that for varying  $\Delta$ , total distortion is a good proxy for model performance (Figure 6). This relationship holds across tasks (see Appendix B.5).

Alternatively to (2), we can place a limit on distortion while minimizing the rate. In either case, the global optimum may be found by minimizing the Lagrangian  $L(\mathcal{Q}, \lambda) = R(\mathcal{Q}) + \lambda D(\mathcal{Q})$ , where  $\lambda$  is the Lagrange multiplier. In practice,  $\lambda$  is often adjusted until the objective’s hard constraint is satisfied. This is a well-studied problem in lossy data compression (Cover & Thomas, 2006, Chapter 10.7), and due to the separability of both terms across updates, is reminiscent of the principle of Pareto efficiency, where  $\mathcal{Q}$  represents a mode of resource allocation. Due to this separability, the optimal policy yielding quantization step sizes  $\Delta_t^k = \mathcal{Q}(\lambda, u_t^k)$  can be found in a distributed way: while  $\lambda$  is chosen centrally, each client solves the problem

$$\Delta_t^k = \arg \min_{\delta} |\mathcal{E}(u_t^k, \delta)| + \lambda \|u_t^k - \mathcal{D}(\mathcal{E}(u_t^k, \delta), \delta)\|_2^2. \quad (4)$$

However, this can place an unacceptable computational burden on the clients, which leads to the following experiment.

**Experiment.** For varying  $\lambda$ , we let clients solve (4) by brute force, selecting from a pre-determined set of  $\delta$ ’s. We observe significant agreement on  $\Delta_t^k$  across clients and rounds for any given  $\lambda$  (Figure 7). That is, empirically,  $\Delta_t^k$  is largely independent of  $u_t^k$ , and there is a monotonic relationship between  $\Delta_t^k$  and  $\lambda$ . Further, we find that this

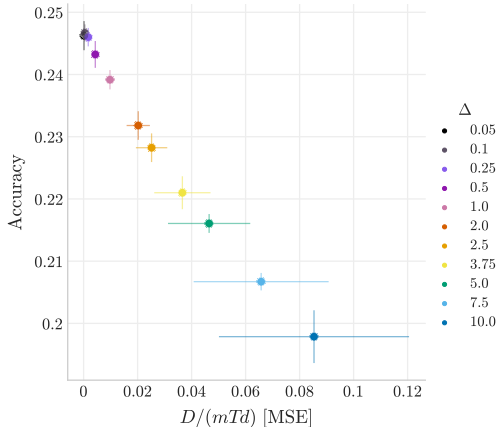


Figure 6. Accuracy of a model versus average per-coordinate distortion for various quantization step sizes  $\Delta$  on Stack Overflow NWP. Error bars indicate the variance over 5 random trials.

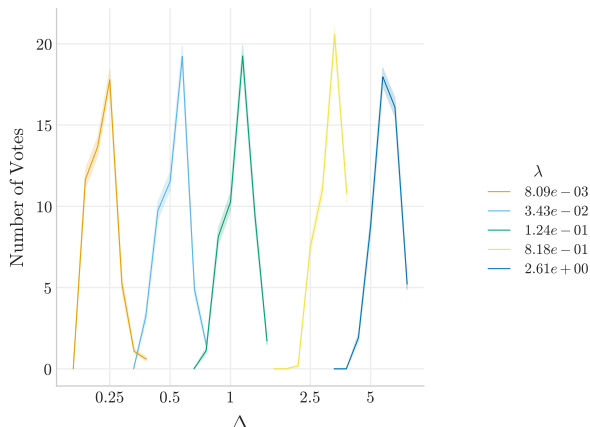


Figure 7. Histogram of client-selected quantization step sizes  $\Delta_t^k$  for a given  $\lambda$ , averaged across training rounds, on Stack Overflow NWP.

relationship is even consistent across different architectures, tasks, and optimizers (Appendix B.6, Figure 8).

Thus, we can set  $\mathcal{Q}(\lambda, u_t^k) \equiv \Delta$ , and let the server control a global  $\Delta$  rather than  $\lambda$ , eliminating a hyperparameter and the need to solve (4) on the client side. Our method is thus remarkably simple and almost completely described by Algorithm 2. It has only one global hyperparameter  $\Delta$  which needs to be adjusted until the desired trade-off between total bitrate budget and model performance is met. The choice of this hyperparameter is relatively predictable, due to the consistency across tasks and optimizers. A similar relationship between quantization step size and the Lagrange parameter is exploited in contemporary video compression methods, where quantization must be controlled across video frames (Sullivan & Wiegand, 1998).

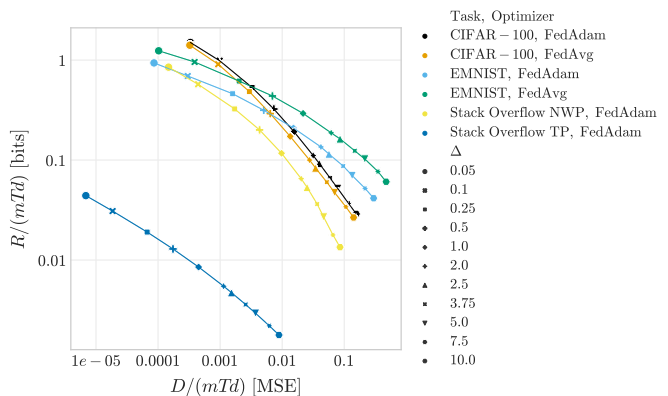


Figure 8. Even though different model architectures tend to have differing  $R$ - $D$  frontiers, a given choice of  $\Delta$  tends to correspond to approximately the same value of  $\lambda$  (which is related to the slope of the curve at that point).

### 3. Experimental Setup

In order to inform our design choices above, we perform empirical evaluations of Algorithm 1 on a variety of federated tasks drawn from benchmarks in (Reddi et al., 2021).<sup>3</sup>

**Datasets, Models, and Tasks.** We use three datasets: CIFAR-100 (Krizhevsky, 2009), EMNIST (Cohen et al., 2017), and Stack Overflow (Authors, 2019c). For CIFAR-100, we use the artificial client partition proposed by Reddi et al. (2021). The other two datasets have natural client partitions where each client is an author (of handwritten digits and forum posts). For CIFAR-100, we train a ResNet-18, replacing batch normalization with group normalization (see (Hsieh et al., 2020)). For EMNIST, we train a network with two convolutional layers, max-pooling, dropout, and two dense layers. For Stack Overflow, we perform next-word prediction (NWP) using an RNN with a single LSTM layer, and tag prediction (TP) using a multi-class logistic regression model. For full details, see Appendix A.1.

**Algorithms.** We focus on two special cases of Algorithm 1: FedAvg (McMahan et al., 2017) and FedAdam (Reddi et al., 2021). In both, LOCALTRAIN is  $E$  epochs of mini-batch SGD with client learning rate  $\eta_c$ . For FedAvg and FedAdam, SERVERUPDATE is SGD or Adam (respectively) with server learning rate  $\eta_s$ . We use FedAvg and FedAdam on the vision tasks (CIFAR-100 and EMNIST), but only FedAdam on the language tasks (Stack Overflow), as FedAvg performs poorly there (Reddi et al., 2021). We set  $E = 1$  and use a batch size of 32 throughout. We perform  $T = 1500$  rounds of training for each task. At each round, we sample  $m = 50$  clients uniformly at random. We tune  $\eta_c, \eta_s$  over

<sup>3</sup>Code available at: [https://github.com/google-research/federated/tree/1b31b84/compressed\\_communication](https://github.com/google-research/federated/tree/1b31b84/compressed_communication)

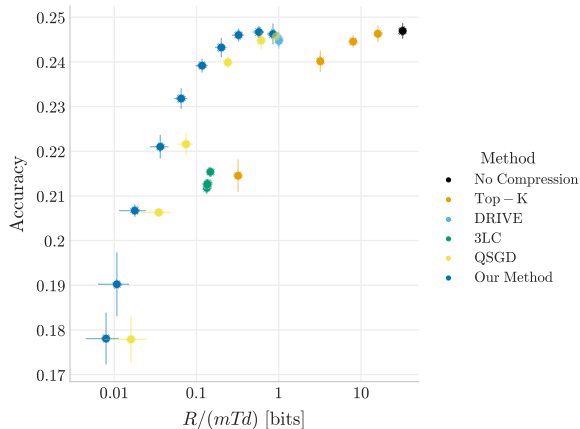


Figure 9. Final model accuracy versus per-coordinate bit rate for a variety of methods on Stack Overflow NWP. Error bars indicate variance in average per-coordinate rate and final model accuracy over 5 random trials.

$\{10^{-3}, 10^{-2}, \dots, 10\}$  by selecting the values that minimize the average validation loss over 5 random trials.

**Other Benchmarks.** We evaluate Algorithm 1 with our compression method and existing compression methods on the tasks described above (results in Figure 9). As a baseline, we include runs with NOCOMPRESSION, where  $(\mathcal{E}, \mathcal{D})$  are no-ops and clients communicate their weighted updates at 32-bit precision. The accuracy achieved with NOCOMPRESSION can be understood as the target accuracy we aim to reach with compression. We also compare to TOP-K (Aji & Heafield, 2017), DRIVE (Vargaftik et al., 2021), 3LC (Lim et al., 2019), and QSGD (Alistarh et al., 2017). For details on these methods, see Appendix A.2.

Notable methods we do not compare with include FEDSKETCH (Haddadpour et al., 2020), 1BITSGD (Seide et al., 2014), and TERNGRAD (Wen et al., 2017). The first two use error-correction mechanisms which do not comply with our stateless requirement, while the latter two are often outperformed by QSGD, and can suffer in performance when client updates are unevenly distributed (Xu et al., 2020).

## 4. Discussion

Compared to the benchmarks above, our method is highly competitive. In most cases our method outperforms all others in terms of the accuracy–rate trade-off, as demonstrated in Figure 9. For those few cases in which our method does not raise the accuracy–communication cost frontier, we match the performance of the best existing methods to which we compare. Plots of overall performance on the other tasks are included in Appendix B.7.

The poor performance of 3LC can be attributed to the use of stochastic rounding in place of error correction. TOP-

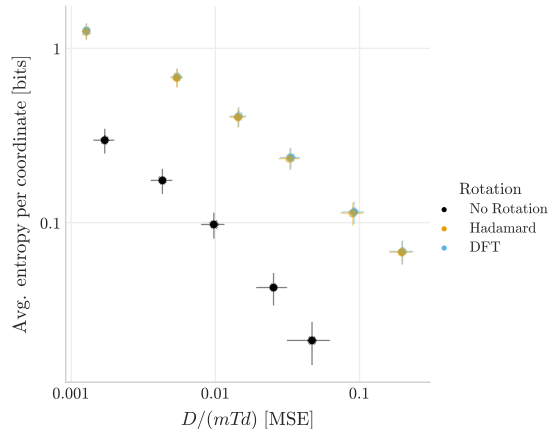


Figure 10. Average per-coordinate entropy versus distortion of client updates in Stack Overflow NWP, after a random rotation (or no rotation) is applied. Error bars indicate the variance across 5 random trials.

K’s accuracy is highly dependent on the sparsity of client updates, and with a fixed dimension it does not achieve impressive compression ratios. DRIVE and QSGD are most competitive with our method. The key distinguishing feature of DRIVE is their use of random rotations. For QSGD the key differentiating factor is normalization, which leads to a different effective  $\Delta$  per update. We focus on each of these design choices in the ablation studies that follow.

**Ablation: Random Rotations.** Random rotations have been used in fixed-rate federated compression methods by Konečný et al. (2016), Suresh et al. (2017), and Vargaftik et al. (2021). Suresh et al. (2017) motivate using fixed-rate compression for compatibility with secure aggregation (Bonawitz et al., 2017) and Vargaftik et al. (2021) argue that variable-length encodings are expensive to compute. While using a fixed-bit code in combination with a uniform quantizer on a heavy-tailed distribution is highly inefficient from an entropy coding standpoint, applying a random rotation to the input distribution before quantization will ameliorate this effect, as it will “Gaussianize” the distribution.

However, this can hide the existing structure of the model updates; it increases the per-coordinate entropy, and hence the expected bitrate (recall that a Gaussian is the max-entropy distribution for a given variance). Figure 10 shows that applying a random Hadamard or DFT rotation before quantization results in a worse entropy–distortion frontier than if quantization is applied in the original coordinate space. Even using a random rotation fixed throughout training produces higher entropy marginal distributions, indicating that  $u_t^k$  is already in a suitable coordinate system for compression (Figure 11).

As we show in Appendix B.8, for Stack Overflow and EMNIST tasks, the entropy–distortion frontier is significantly

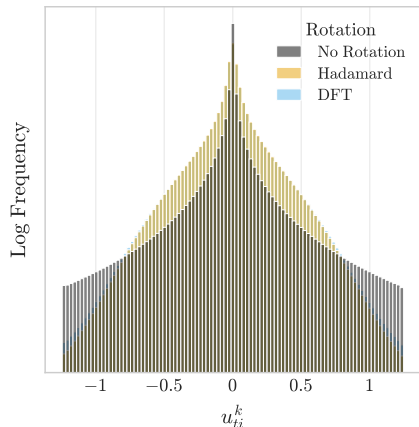


Figure 11. Histogram of client update coordinates in Stack Overflow NWP after applying a fixed, randomly sampled rotation (or no rotation). Frequencies are averaged across rounds.

better in the original space than after applying random rotations. The frontier is only slightly better for the CIFAR-100 task. This intuitively makes sense, as the CIFAR-100 client updates are not as sparse as in other tasks; the sparsity is observed primarily in the output, as nearly all clients only have a fraction of the possible image labels.

**Ablation: Normalization.** Distributed training compression methods (e.g., Alistarh et al., 2017; Vargaftik et al., 2021) often scale each client update to have the same vector magnitude  $\|u_t^k\|$  before applying compression. This is equivalent to choosing a magnitude-dependent per-client  $\Delta_t^k$ . However, as we show in Section 2.3, each client should quantize their update to the same fidelity, since other choices lead to an inferior global rate–distortion trade-off. This is the key differentiator between QSGD and our method.

For optimization in heterogeneous settings (Li et al., 2020), the update magnitudes can vary dramatically. Comparing the  $R$ – $D$  curves for our method and QSGD, we find that our method provides a better rate–distortion performance, particularly on tasks with significant client heterogeneity (Figure 12). When client updates are more homogeneous (as in the CIFAR-100 dataset, where each client has the same number of examples (Reddi et al., 2021)), gains are, as expected, negligible. The normalization strategy of QSGD thus may be the reason why our method performs better.

## 5. Outlook and Conclusions

An additional improvement over the results reported above is possible noting that higher levels of distortion are less problematic in earlier rounds, and more so later on, as the training gets closer to convergence. Formally, this is analogous to the fact that for SGD, the variance of the stochastic gradient determines the convergence radius of its iter-

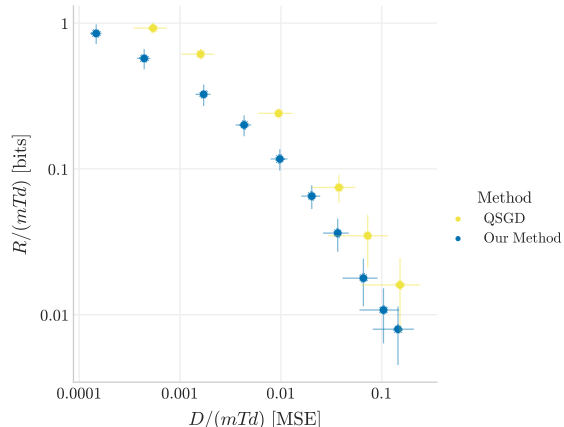


Figure 12. Average per-coordinate rate versus distortion of client updates in Stack Overflow NWP for QSGD and our method. Error bars indicate variance over 5 random trials.

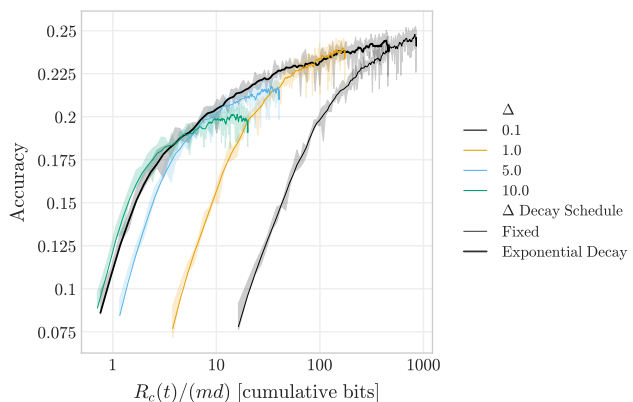


Figure 13. Validation accuracy versus cumulative bitrate for our method with fixed  $\Delta$  and exponentially decayed  $\Delta$  on Stack Overflow NWP.

ates (Alistarh et al., 2017, Theorem 1). Thus, rather than keeping the  $R$ – $D$  trade-off fixed over the course of training, we could vary it over time. As the relationship between  $\Delta$  and  $\lambda$  discussed in Section 2.3 holds across rounds, one simple way to do this is to decay  $\Delta$ .

To test this idea, we applied an exponential decay schedule on  $\Delta$  (details in Appendix B.10; one result in Figure 13). Training with large  $\Delta$  is communication-efficient at first, but accuracy saturates quickly. Training with small  $\Delta$  reaches top accuracy, but at the expense of communication. With  $\Delta$  decay, top accuracy is reached with overall fewer bits transmitted. We found comparable results across other tasks and optimizers (Appendix B.10), but did not tune the schedules. More sophisticated ways of modulating the  $R$ – $D$  trade-off over time are conceivable, such as adapting to running training metrics, but would exceed the scope of this paper.

As shown earlier, our compression method performs better

than existing methods in the cross-device FL setting, even at a fixed  $R$ – $D$  trade-off, over a wide range of tasks and optimizers. We accomplish this with a simple stateless algorithm that produces a variable-length encoding, tailored to the empirical distribution of client updates. We explicitly introduce rate–distortion optimization into federated learning, which guides our choice of per-client encoding parameters, and as shown in the paragraph above, may lead to further improvements. Another topic of future work is to explore compatibility with privacy protocols.

## References

- Aji, A. F. and Heafield, K. Sparse communication for distributed gradient descent. In *Proceedings of the 2017 Conference on Empirical Methods in Natural Language Processing*, pp. 440–445, 2017.
- Albasyoni, A., Safaryan, M., Condat, L., and Richtárik, P. Optimal gradient compression for distributed and federated learning. *arXiv preprint arXiv:2010.03246*, 2020.
- Alistarh, D., Grubic, D., Li, J., Tomioka, R., and Vojnovic, M. QSGD: Communication-efficient SGD via gradient quantization and encoding. *Advances in Neural Information Processing Systems*, 30:1709–1720, 2017.
- Authors, T. T. TensorFlow Federated, 2019a. URL <https://www.tensorflow.org/federated>.
- Authors, T. T. F. TensorFlow Federated CIFAR-100 dataset, 2019b. URL [https://www.tensorflow.org/federated/api\\_docs/python/tff/simulation/datasets/cifar100/load\\_data](https://www.tensorflow.org/federated/api_docs/python/tff/simulation/datasets/cifar100/load_data).
- Authors, T. T. F. TensorFlow Federated Stack Overflow dataset, 2019c. URL [https://www.tensorflow.org/federated/api\\_docs/python/tff/simulation/datasets/stackoverflow/load\\_data](https://www.tensorflow.org/federated/api_docs/python/tff/simulation/datasets/stackoverflow/load_data).
- Beznosikov, A., Horváth, S., Richtárik, P., and Safaryan, M. On biased compression for distributed learning. *arXiv preprint arXiv:2002.12410*, 2020.
- Bonawitz, K., Ivanov, V., Kreuter, B., Marcedone, A., McMahan, H. B., Patel, S., Ramage, D., Segal, A., and Seth, K. Practical secure aggregation for privacy-preserving machine learning. In *proceedings of the 2017 ACM SIGSAC Conference on Computer and Communications Security*, pp. 1175–1191, 2017.
- Bonawitz, K., Eichner, H., Grieskamp, W., Huba, D., Ingerman, A., Ivanov, V., Kiddon, C., Konečný, J., Mazzocchi, S., McMahan, B., Van Overveldt, T., Petrou, D., Ramage, D., and Roselander, J. Towards federated learning at scale: System design. In Talwalkar, A., Smith, V., and Zaharia, M. (eds.), *Proceedings of Machine Learning and Systems*, volume 1, pp. 374–388, 2019. URL <https://proceedings.mlsys.org/paper/2019/file/bd686fd640be98efaae0091fa301e613-Paper.pdf>.
- Cohen, G., Afshar, S., Tapson, J., and Van Schaik, A. EMNIST: Extending MNIST to handwritten letters. In *2017 International Joint Conference on Neural Networks (IJCNN)*, pp. 2921–2926. IEEE, 2017.
- Cover, T. M. and Thomas, J. A. *Elements of Information Theory*. Wiley, 2 edition, 2006. ISBN 978-0-471-24195-9.
- Elias, P. Universal codeword sets and representations of the integers. *IEEE Trans. on Information Theory*, 21(2), 1975. doi: 10.1109/TIT.1975.1055349.
- Gray, R. M. and Neuhoff, D. L. Quantization. *IEEE Trans. on Information Theory*, 44(6), 1998. doi: 10.1109/18.720541.
- Haddadpour, F., Karimi, B., Li, P., and Li, X. FedSketch: Communication-efficient and private federated learning via sketching. *arXiv preprint arXiv:2008.04975*, 2020.
- Haddadpour, F., Kamani, M. M., Mokhtari, A., and Mahdavi, M. Federated learning with compression: Unified analysis and sharp guarantees. In *International Conference on Artificial Intelligence and Statistics*, pp. 2350–2358. PMLR, 2021.
- He, K., Zhang, X., Ren, S., and Sun, J. Deep residual learning for image recognition. In *Proceedings of the IEEE conference on computer vision and pattern recognition*, pp. 770–778, 2016.
- Hochreiter, S. and Schmidhuber, J. Long short-term memory. *Neural Computation*, 9(8):1735–1780, 1997.
- Hsieh, K., Phanishayee, A., Mutlu, O., and Gibbons, P. The non-IID data quagmire of decentralized machine learning. In *Proceedings of the 37th International Conference on Machine Learning*, 2020.
- Huba, D., Nguyen, J., Malik, K., Zhu, R., Rabbat, M., Yousefpour, A., Wu, C.-J., Zhan, H., Ustinov, P., Srinivas, H., et al. Papaya: Practical, private, and scalable federated learning. *arXiv preprint arXiv:2111.04877*, 2021.
- Kairouz, P., McMahan, H. B., Avent, B., Bellet, A., Bennis, M., Bhagoji, A. N., Bonawitz, K., Charles, Z., Cormode, G., Cummings, R., D’Oliveira, R. G. L., Eichner, H., Rouayheb, S. E., Evans, D., Gardner, J., Garrett, Z., Gascón, A., Ghazi, B., Gibbons, P. B., Gruteser, M.,

- Harchaoui, Z., He, C., He, L., Huo, Z., Hutchinson, B., Hsu, J., Jaggi, M., Javidi, T., Joshi, G., Khodak, M., Konečný, J., Korolova, A., Koushanfar, F., Koyejo, S., Lepoint, T., Liu, Y., Mittal, P., Mohri, M., Nock, R., Özgür, A., Pagh, R., Qi, H., Ramage, D., Raskar, R., Raykova, M., Song, D., Song, W., Stich, S. U., Sun, Z., Suresh, A. T., Tramèr, F., Vepakomma, P., Wang, J., Xiong, L., Xu, Z., Yang, Q., Yu, F. X., Yu, H., and Zhao, S. Advances and open problems in federated learning. *Foundations and Trends® in Machine Learning*, 14(1–2):1–210, 2021. ISSN 1935-8237. doi: 10.1561/22000000083. URL <http://dx.doi.org/10.1561/22000000083>.
- Konečný, J., McMahan, H. B., Yu, F. X., Richtárik, P., Suresh, A. T., and Bacon, D. Federated learning: Strategies for improving communication efficiency. *arXiv preprint arXiv:1610.05492*, 2016.
- Krizhevsky, A. Learning multiple layers of features from tiny images. Technical report, 2009.
- Li, T., Sahu, A. K., Zaheer, M., Sanjabi, M., Talwalkar, A., and Smith, V. Federated optimization in heterogeneous networks. In Dhillon, I. S., Papailiopoulos, D. S., and Sze, V. (eds.), *Proceedings of Machine Learning and Systems 2020, MLSys 2020, Austin, TX, USA, March 2-4, 2020*. mlsys.org, 2020. URL <https://proceedings.mlsys.org/book/316.pdf>.
- Li, W. and McCallum, A. Pachinko allocation: DAG-structured mixture models of topic correlations. In *Proceedings of the 23rd International Conference on Machine Learning*, 2006.
- Lim, H., Andersen, D. G., and Kaminsky, M. 3LC: Lightweight and effective traffic compression for distributed machine learning. In Talwalkar, A., Smith, V., and Zaharia, M. (eds.), *Proceedings of Machine Learning and Systems*, volume 1, pp. 53–64, 2019. URL <https://proceedings.mlsys.org/paper/2019/file/6364d3f0f495b6ab9dcf8d3b5c6e0b01-Paper.pdf>.
- Lin, Y., Han, S., Mao, H., Wang, Y., and Dally, B. Deep gradient compression: Reducing the communication bandwidth for distributed training. In *International Conference on Learning Representations*, 2018. URL <https://openreview.net/forum?id=SkhQHMWOW>.
- Liu, Y., Fan, T., Chen, T., Xu, Q., and Yang, Q. Fate: An industrial grade platform for collaborative learning with data protection. *Journal of Machine Learning Research*, 22(226):1–6, 2021. URL <http://jmlr.org/papers/v22/20-815.html>.
- Ludwig, H., Baracaldo, N., Thomas, G., Zhou, Y., Anwar, A., Rajamoni, S., Ong, Y., Radhakrishnan, J., Verma, A., Sinn, M., et al. Ibm federated learning: an enterprise framework white paper v0. 1. *arXiv preprint arXiv:2007.10987*, 2020.
- McMahan, B., Moore, E., Ramage, D., Hampson, S., and Arcas, B. A. y. Communication-Efficient Learning of Deep Networks from Decentralized Data. In Singh, A. and Zhu, J. (eds.), *Proceedings of the 20th International Conference on Artificial Intelligence and Statistics*, volume 54 of *Proceedings of Machine Learning Research*, pp. 1273–1282. PMLR, 20–22 Apr 2017. URL <https://proceedings.mlr.press/v54/mcmahan17a.html>.
- Mikolov, T., Karafiát, M., Burget, L., Černocký, J., and Khudanpur, S. Recurrent neural network based language model. In *Eleventh Annual Conference of the International Speech Communication Association*, 2010.
- Reddi, S. J., Charles, Z., Zaheer, M., Garrett, Z., Rush, K., Konečný, J., Kumar, S., and McMahan, H. B. Adaptive federated optimization. In *International Conference on Learning Representations*, 2021.
- Reisizadeh, A., Mokhtari, A., Hassani, H., Jadbabaie, A., and Pedarsani, R. FedPAQ: A communication-efficient federated learning method with periodic averaging and quantization. In *International Conference on Artificial Intelligence and Statistics*, pp. 2021–2031. PMLR, 2020.
- Rothchild, D., Panda, A., Ullah, E., Ivkin, N., Stoica, I., Braverman, V., Gonzalez, J., and Arora, R. FetchSGD: Communication-efficient federated learning with sketching. In *International Conference on Machine Learning*, pp. 8253–8265. PMLR, 2020.
- Sattler, F., Wiedemann, S., Müller, K.-R., and Samek, W. Robust and communication-efficient federated learning from non-IID data. *IEEE transactions on neural networks and learning systems*, 31(9):3400–3413, 2019.
- Schuchman, L. Dither signals and their effect on quantization noise. *IEEE Transactions on Communication Technology*, 12(4):162–165, December 1964.
- Seide, F., Fu, H., Droppo, J., Li, G., and Yu, D. 1-bit stochastic gradient descent and its application to data-parallel distributed training of speech DNNs. In *Fifteenth Annual Conference of the International Speech Communication Association*, 2014.
- Shannon, C. E. A mathematical theory of communication. *The Bell System Technical Journal*, 27(3):379–423, 1948. doi: 10.1002/j.1538-7305.1948.tb01338.x.

- Sullivan, G. J. and Wiegand, T. Rate–distortion optimization for video compression. *IEEE Signal Processing Magazine*, 15(6), 1998. doi: 10.1109/79.733497.
- Suresh, A. T., Felix, X. Y., Kumar, S., and McMahan, H. B. Distributed mean estimation with limited communication. In *International Conference on Machine Learning*, pp. 3329–3337. PMLR, 2017.
- Vargaftik, S., Basat, R. B., Portnoy, A., Mendelson, G., Ben-Itzhak, Y., and Mitzenmacher, M. Drive: One-bit distributed mean estimation. *arXiv preprint arXiv:2105.08339*, 2021.
- Vogels, T., Karimireddy, S. P., and Jaggi, M. PowerSGD: Practical low-rank gradient compression for distributed optimization. *Advances in Neural Information Processing Systems*, 32:14259–14268, 2019.
- Wang, H., Sievert, S., Liu, S., Charles, Z., Papailiopoulos, D., and Wright, S. Atomo: Communication-efficient learning via atomic sparsification. *Advances in Neural Information Processing Systems*, 31:9850–9861, 2018.
- Wang, J., Charles, Z., Xu, Z., Joshi, G., McMahan, H. B., Al-Shedivat, M., Andrew, G., Avestimehr, S., Daly, K., Data, D., et al. A field guide to federated optimization. *arXiv preprint arXiv:2107.06917*, 2021.
- Wen, W., Xu, C., Yan, F., Wu, C., Wang, Y., Chen, Y., and Li, H. Terngrad: Ternary gradients to reduce communication in distributed deep learning. *Advances in Neural Information Processing Systems*, 30, 2017.
- Wu, Y. and He, K. Group normalization. In *Proceedings of the European Conference on Computer Vision (ECCV)*, pp. 3–19, 2018.
- Xu, H., Ho, C.-Y., Abdelmoniem, A. M., Dutta, A., Bergou, E. H., Karatsenidis, K., Canini, M., and Kalnis, P. Compressed communication for distributed deep learning: Survey and quantitative evaluation. Technical report, 2020.

## A. Full Experimental Details

### A.1. Datasets, Tasks and Models

We use three datasets throughout our work: CIFAR-100 (Krizhevsky, 2009), the federated extended MNIST dataset (EMNIST) (Cohen et al., 2017), and the Stack Overflow dataset (Authors, 2019c). The first two datasets are image datasets, the last is a language dataset. All datasets are publicly available. We specifically use the versions available in TensorFlow Federated (Authors, 2019a), which gives a federated structure to all three datasets.

For a summary of the dataset statistics, tasks, and models used, see Table 1. We discuss these in more detail below.

Table 1. Datasets, Tasks & Models

DATASET	NUM CLIENTS		NUM EXAMPLES		TASK	MODEL
	TRAIN	TEST	TRAIN	TEST		
EMNIST	3,400	3,400	671,585	77,483	CHARACTER RECOGNITION	CNN
STACK OVERFLOW	342,477	204,088	135.8M	16.6M	NEXT-WORD PREDICTION	LSTM
STACK OVERFLOW	342,477	204,088	135.8M	16.6M	TAG PREDICTION	LOGISTIC REGRESSION
CIFAR-100	500	100	50,000	10,000	IMAGE RECOGNITION	RESNET-18 + GROUPNORM

**CIFAR-100** The CIFAR-100 dataset is a vision dataset consisting of  $32 \times 32 \times 3$  images with 100 possible labels. This dataset does not have a canonical partitioning among clients. However, an artificial partitioning among clients was created by Reddi et al. (2021) using hierarchical latent Dirichlet allocation to obtain moderate amounts of heterogeneity among clients. This partitioning is based on Pachinko allocation (Li & McCallum, 2006), and is available in TensorFlow Federated (Authors, 2019b). Under this partitioning, each client typically has only a subset of the 100 possible labels. The dataset has 500 training clients and 100 test clients, each with 100 examples in their local dataset.

We train a ResNet-18 (He et al., 2016) on this dataset, where we replace all batch normalization layers with group normalization layers (Wu & He, 2018), as group norm can perform better than batch norm in federated settings (Hsieh et al., 2020). We use group normalization layers with two groups. We perform small amounts of data augmentation and preprocessing for each train and test sample. We first centrally crop each image (24, 24, 3). We then normalize the pixel values according to their mean and standard deviation.

**EMNIST** The EMNIST dataset contains  $28 \times 28$  gray-scale pixel images of hand-written alphanumeric characters. There are 62 alphanumeric characters in the dataset, and the characters are partitioned among clients according to their author. The dataset has 3,400 clients, who have both train and test datasets. The dataset has natural heterogeneity stemming from the writing style of each person. We train a convolutional network on the dataset (the same as in (Reddi et al., 2021)). The network uses two convolutional layers (each with  $3 \times 3$  kernels and strides of length 1), followed by a max pooling layer using dropout with  $p = 0.25$ , a dense layer with 128 units and dropout with  $p = 0.5$ , and a final dense output layer.

**Stack Overflow** Stack Overflow is a language dataset consisting of question and answers from the Stack Overflow site. The questions and answers also have associated metadata, including tags. Each client corresponds to a user. The specific train/validation/test split from (Authors, 2019c) has 342,477 train clients, 38,758 validation clients, and 204,088 test clients. Notably, the train clients only have examples from before 2018-01-01 UTC, while the test clients only have examples from after 2018-01-01 UTC. The validation clients have examples with no date restrictions, and all validation examples are held-out from both the test and train sets. We perform two tasks on this dataset: next-word prediction and tag prediction. Both tasks are drawn from (Reddi et al., 2021) and use the same models there.

*Next-Word Prediction:* We use padding and truncation to ensure that each sentence has 20 words. We then represent the sentence as a sequence of indices corresponding to the 10,000 most frequently used words, as well as indices representing padding, out-of-vocabulary words, the beginning of a sentence, and the end of a sentence. We perform next-word prediction on these sequences using an a recurrent neural network (RNN) (Mikolov et al., 2010) that embeds each word in a sentence into a learned 96-dimensional space. It then feeds the embedded words into a single LSTM layer (Hochreiter & Schmidhuber, 1997) of hidden dimension 670, followed by a densely connected softmax output layer. The metric used in the main body is

the accuracy over the 10,000-word vocabulary; it does not include padding, out-of-vocab, or beginning or end of sentence tokens when computing the accuracy.

*Tag Prediction:* We represent each sentence in each client’s local dataset as a bag-of-words vector, normalized to have sum 1, restricting to only the 10,000 most frequently used words in the vocabulary. The tags are represented as binary vectors indicating the presence of a tag in the associated meta-data. We restrict to the 500 most frequently occurring tags. We then use a multi-class logistic regression model for tag prediction, using a one-versus-rest classification strategy.

## A.2. Algorithmic Benchmarks

We evaluate our compression method against existing approaches on the tasks described above. As a baseline, we include runs with NOCOMPRESSION, where  $(\mathcal{E}, \mathcal{D})$  are no-ops and clients communicate their weighted updates at full-precision. This method has fixed rate at 32-bits per coordinate and no distortion. The accuracy achieved with NOCOMPRESSION can be understood as the target accuracy we aim to reach with compression. We also compare with the following methods:

- TOP-K (Aji & Heafield, 2017) is a fixed-dimension sparsification method, where only the  $k\%$  largest magnitude coordinates within each client update are communicated along with a bitmask indicating their position within the tensor. We compare with  $k \in \{1\%, 10\%, 25\%, 50\%\}$ .
- DRIVE (Vargaftik et al., 2021) is a fixed-rate method which is designed to provide worst-case guarantees that bound distortion for any input. DRIVE applies a random rotation, then quantizes each tensor coordinate to a single bit, its sign, and computes a scale factor  $S$ . We compare to DRIVE with a structured random rotation, either the Hadamard Transform or the Discrete Fourier Transform, and we use the unbiased the scale factor  $S = \|x\|_2^2 / \|\mathcal{R}(x)\|_1$ .
- 3LC (Lim et al., 2019) is a variable-length compression method that combines 3-value quantization with sparsification and utilizes lossless coding to represent the quantized tensor components compactly. Though 3LC uses memory to compensate for errors, this approach is not realistic in FL and so we instead use stochastic quantization, as mentioned as an appropriate alternative by Lim et al. (2019). We compare with stochastic quantization 3LC using sparsity factor  $s = \{1.00, 1.50, 1.75, 1.90\}$ .
- QSGD (Alistarh et al., 2017) is a variable-length compression method similar to our own, which combines stochastic quantization with Elias source coding. A key differentiator is that the authors parametrize their quantizer by the number of quantization levels  $s$  rather than the size of each level, and they first *normalize* each client’s update and communicate its norm along with the quantized and encoded tensor, so that the tensor can be descaled after it is dequantized. We compare to QSGD over a range of  $s = \{16, 32, 64, 256, 1024, 2048\}$ .

All code for implementing our method, implementing these benchmarks and launching experiments is available at: [https://github.com/google-research/federated/tree/1b31b84/compressed\\_communication](https://github.com/google-research/federated/tree/1b31b84/compressed_communication).

Other notable existing gradient compression methods include 1BITSGD (Seide et al., 2014), TERNGRAD (Wen et al., 2017) and FEDSKETCH (Haddadpour et al., 2020). We omit a direct comparison with 1BITSGD as this method includes error correction and other techniques have been demonstrated to outperform it (Alistarh et al., 2017). We also omit reference to TERNGRAD as it often behaves comparably to or worse than QSGD in practice (Xu et al., 2020), and is actually equivalent to QSGD if the number of quantization levels  $s$ , is set to  $\|g\|_2 / \|g\|_\infty$  (Wang et al., 2018). TERNGRAD’s 3-value quantization also resembles 3LC, which yields a more compact representation (Lim et al., 2019). Xu et al. (2020) note that TERNGRAD performs best when the gradient components are evenly distributed, which is not the case in our FL settings. We omit a direct comparison with FEDSKETCH as the error correction used in this method does not comply with our stateless requirement.

## B. Full Results

### B.1. Histograms

The same experiment as in Figure 1, with other tasks and optimizers. We observe a relatively consistent statistical structure across all tasks: client updates tend to resemble a symmetric power law distribution with a spike at zero. We observe that the CIFAR-100 client updates are significantly less sparse than for the other tasks. Additionally, the Stack Overflow tag prediction client updates are more heavily negative; this asymmetry can be attributed to the infrequency of tags on each client when using many-output logistic regression.

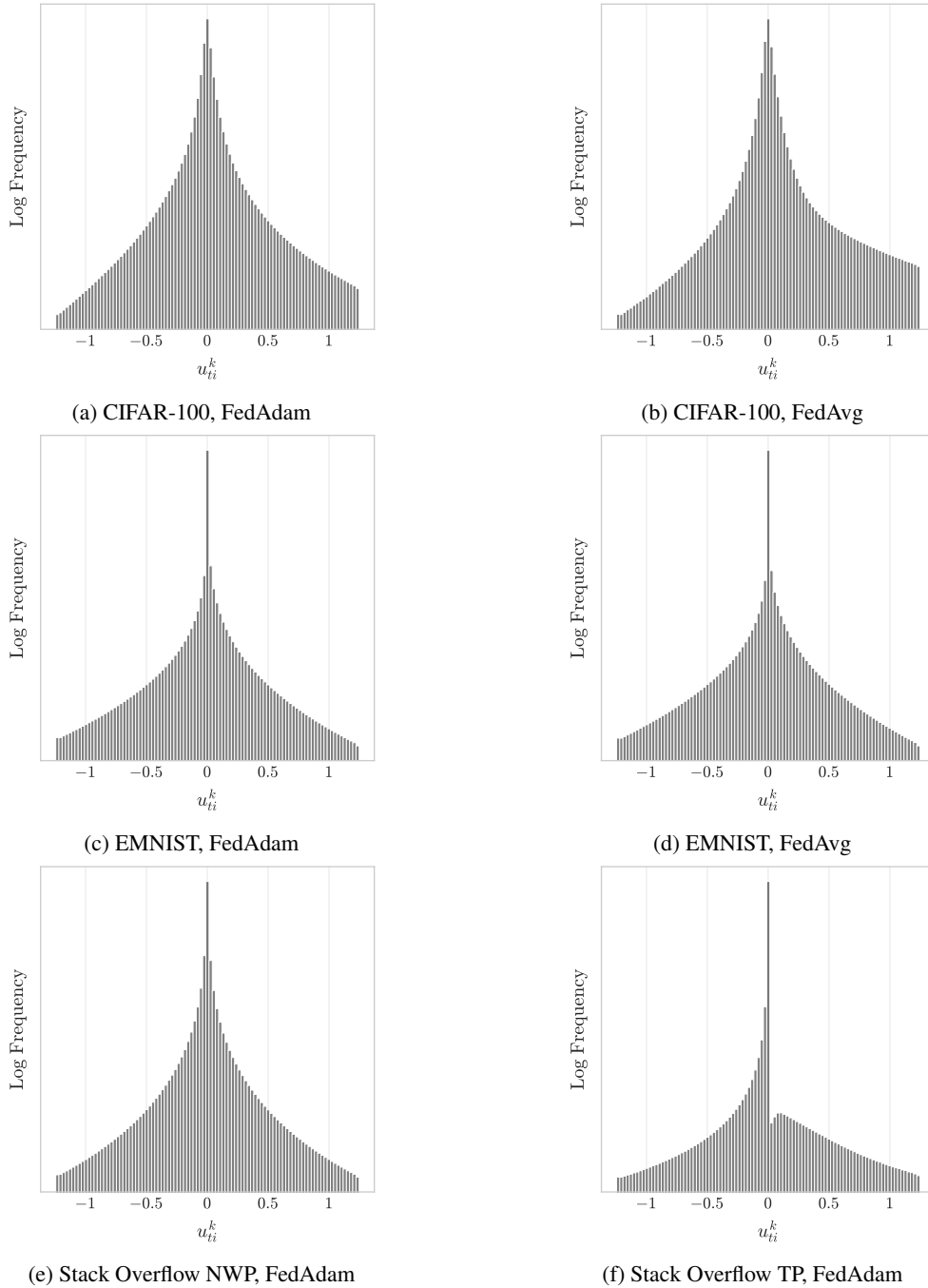


Figure 14. The histograms of weighted client updates averaged over the course of training across tasks and optimizers tend to resemble a symmetric power law distribution with a spike at zero. Notably, the CIFAR-100 client updates are significantly less sparse. The Stack Overflow TP client updates are more heavily negative due to the infrequency of tags on each client.

### B.2. Rounding Methods

The same experiment as in Figure 2, with other tasks and optimizers. We find that regardless of task and optimizer, across quantization step sizes  $\Delta$ , STOCHASTICROUND performs best.

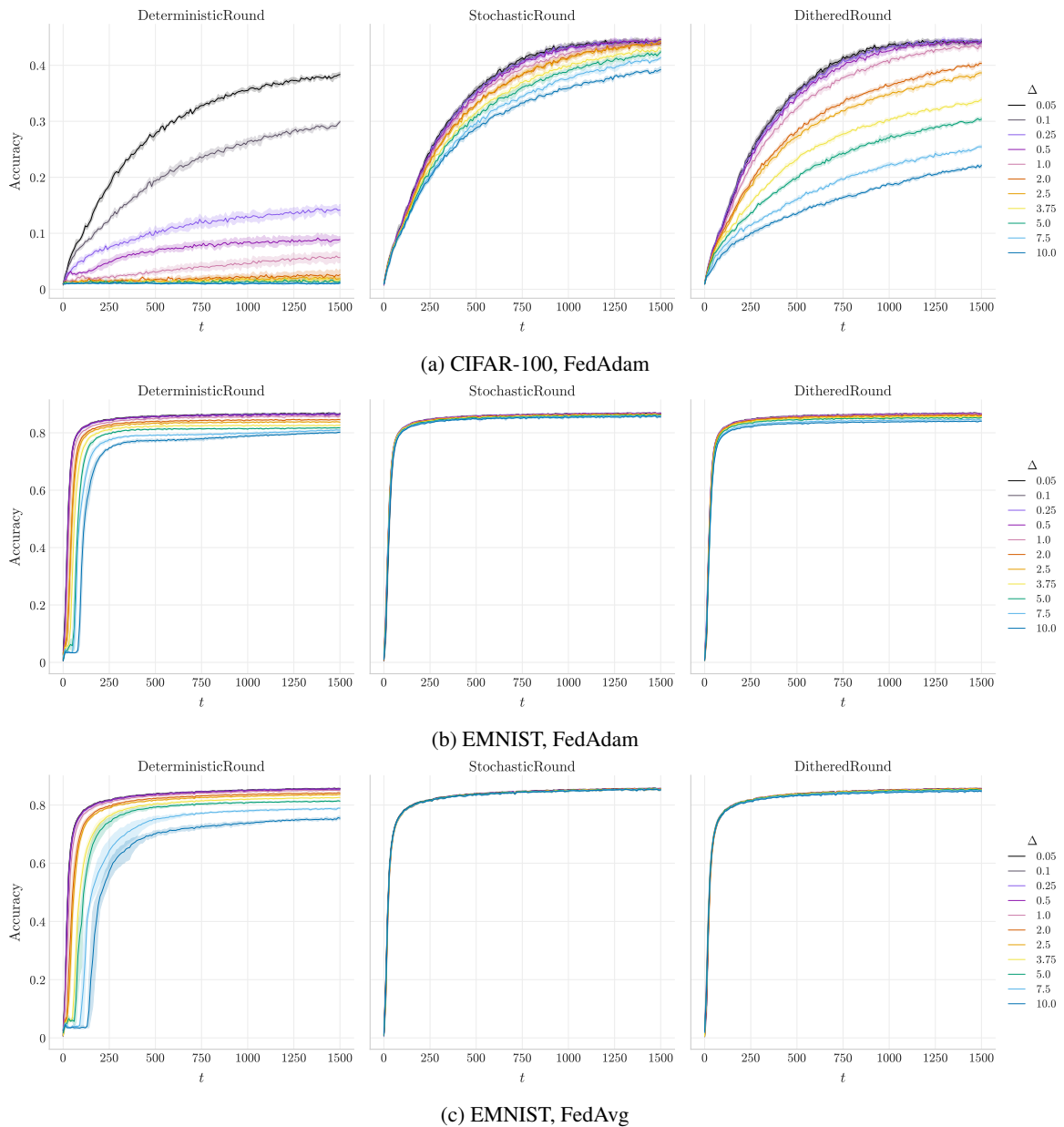
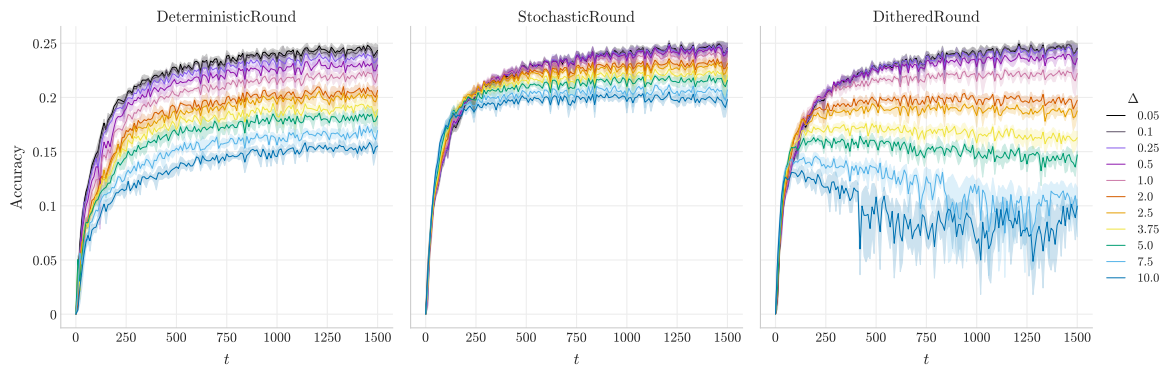
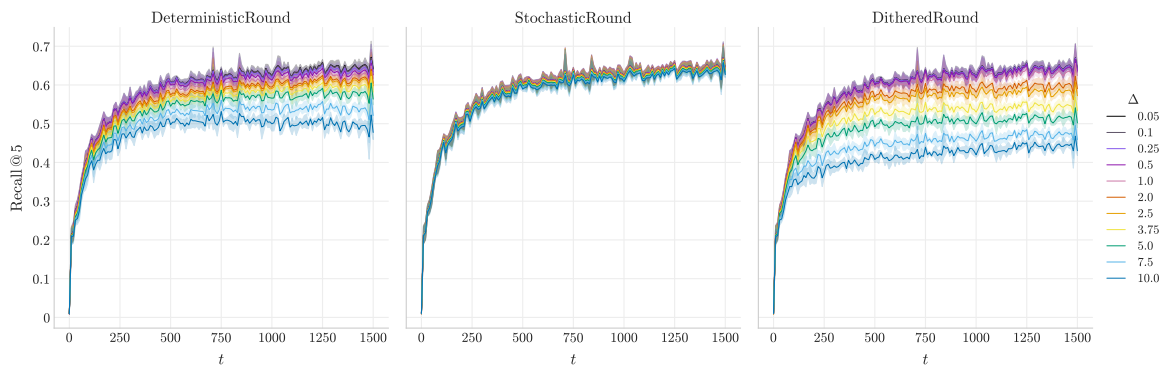


Figure 15. Accuracy over the course of training across quantization step sizes and rounding methods. We find STOCHASTICROUND to perform best across tasks.



(d) Stack Overflow NWP, FedAdam



(e) Stack Overflow TP, FedAdam

Figure 15. Accuracy over the course of training across quantization step sizes and rounding methods. We find STOCHASTICROUND to perform best across tasks. (cont.)

### B.3. Sparsity

The same experiment as in Figure 4, with other tasks and optimizers. We observe relatively high levels of sparsity across all tasks. However, the CIFAR-100 client updates are significantly less sparse than for the other tasks.

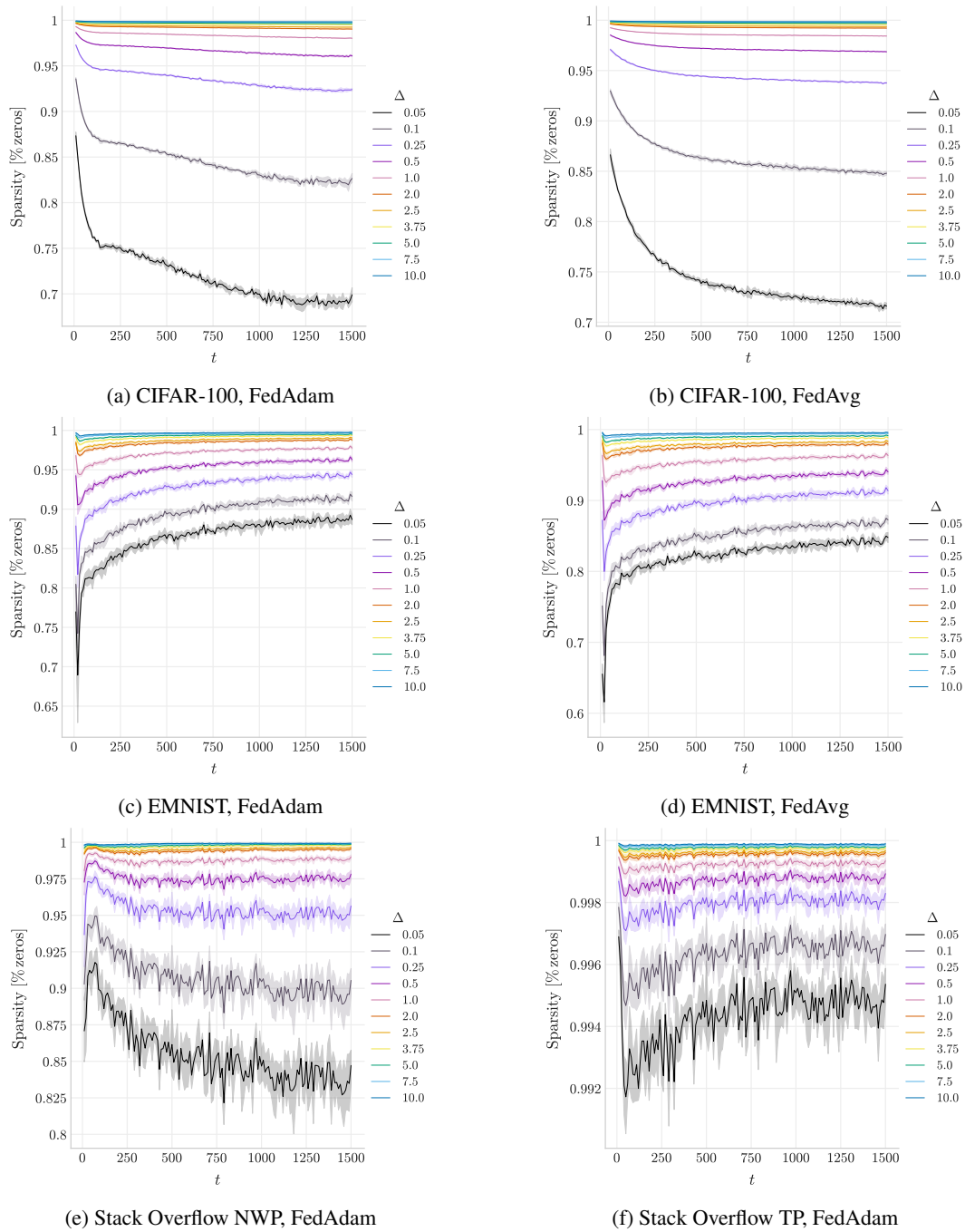
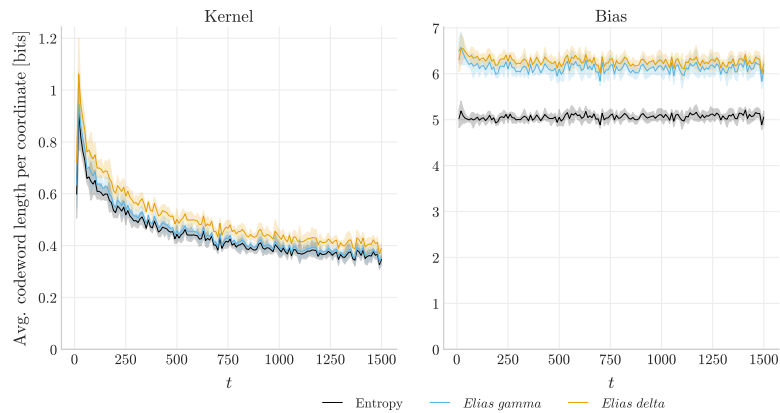


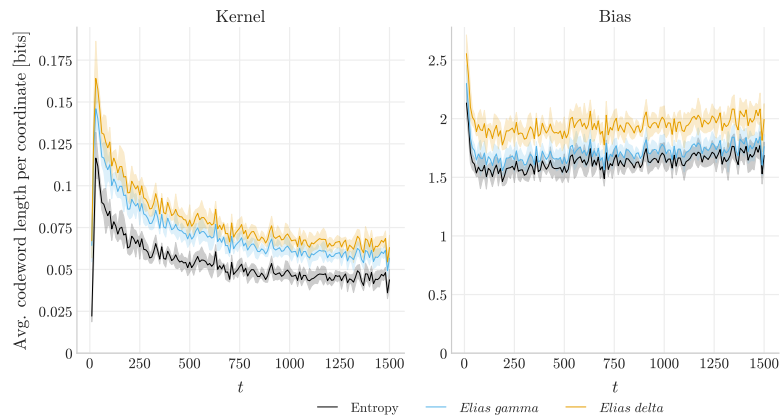
Figure 16. Average sparsity of quantized client updates across step sizes.

### B.4. Universal Code Overhead

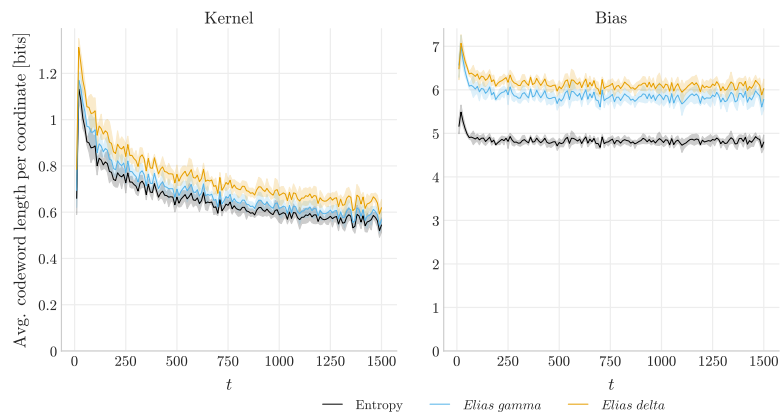
The same experiment as in Figure 5, with additional tasks and values of  $\Delta$ . We find that the *Elias gamma* code consistently outperforms the *Elias delta* code with an acceptable overhead over the entropy of the quantized non-zero magnitudes across values of  $\Delta$  for both the EMNIST character recognition and Stack Overflow next-word prediction tasks.



(a) EMNIST, FedAdam,  $\Delta = 0.05$

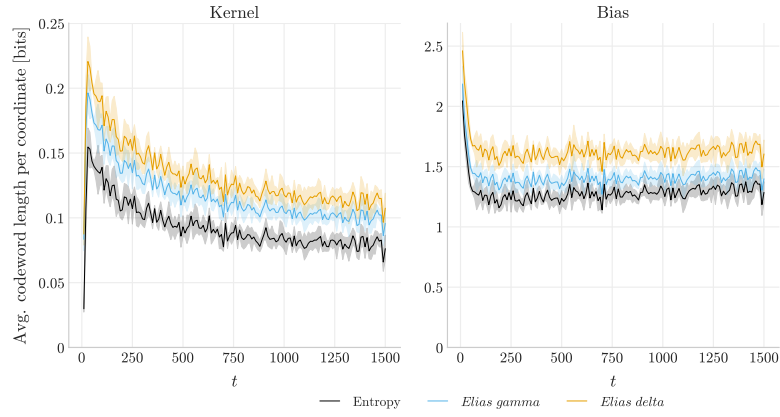


(b) EMNIST, FedAdam,  $\Delta = 0.5$

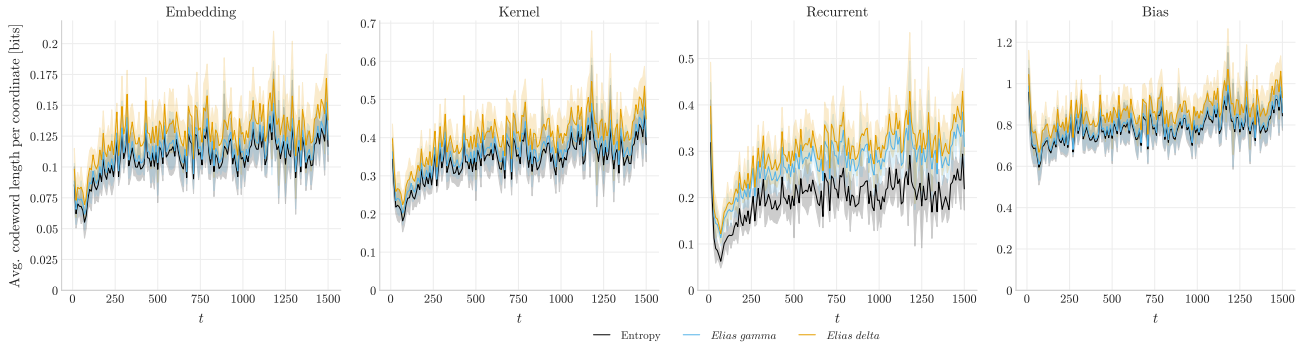


(c) EMNIST, FedAvg,  $\Delta = 0.05$

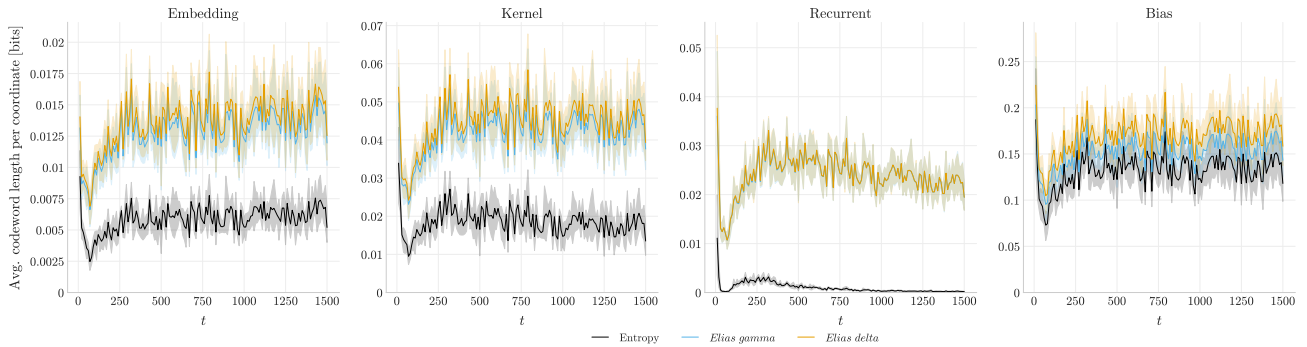
Figure 17. Encoding the magnitude of quantized client updates using the *Elias gamma* and *Elias delta* codes results in an acceptable overhead over the entropy of the data throughout training across different model layer types.



(d) EMNIST, FedAvg,  $\Delta = 0.5$



(e) Stack Overflow NWP, FedAdam,  $\Delta = 0.05$



(f) Stack Overflow NWP, FedAdam,  $\Delta = 0.5$

Figure 17. Encoding the magnitude of quantized client updates using the *Elias gamma* and *Elias delta* codes results in an acceptable overhead over the entropy of the data throughout training across different model layer types. (cont.)

### B.5. Distortion–Accuracy

The same experiment as in Figure 6, with other tasks and optimizers, showing how distortion is a good proxy for accuracy across the board.

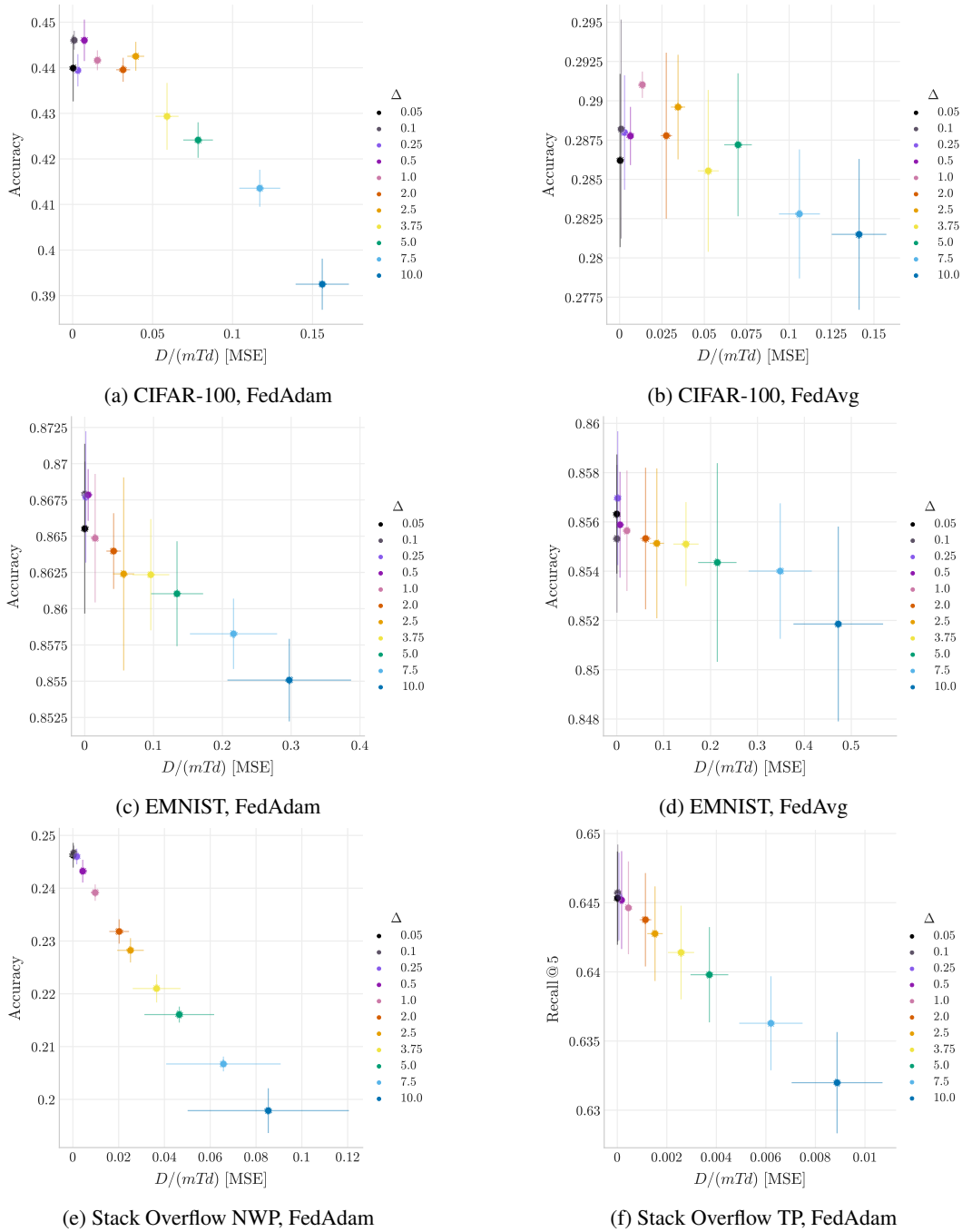


Figure 18. Distortion is a good proxy for the final accuracy of a trained model. Error bars indicate variance in average per-coordinate distortion and final accuracy over five random trials.

### B.6. Client R-D Optimization Experiments

The same experiment as in Figure 7, with other tasks and optimizers. We find that to minimize their local rate–distortion objective specified by the given  $\lambda$ , clients select a consistent quantization step size  $\Delta$  across all our experiments.

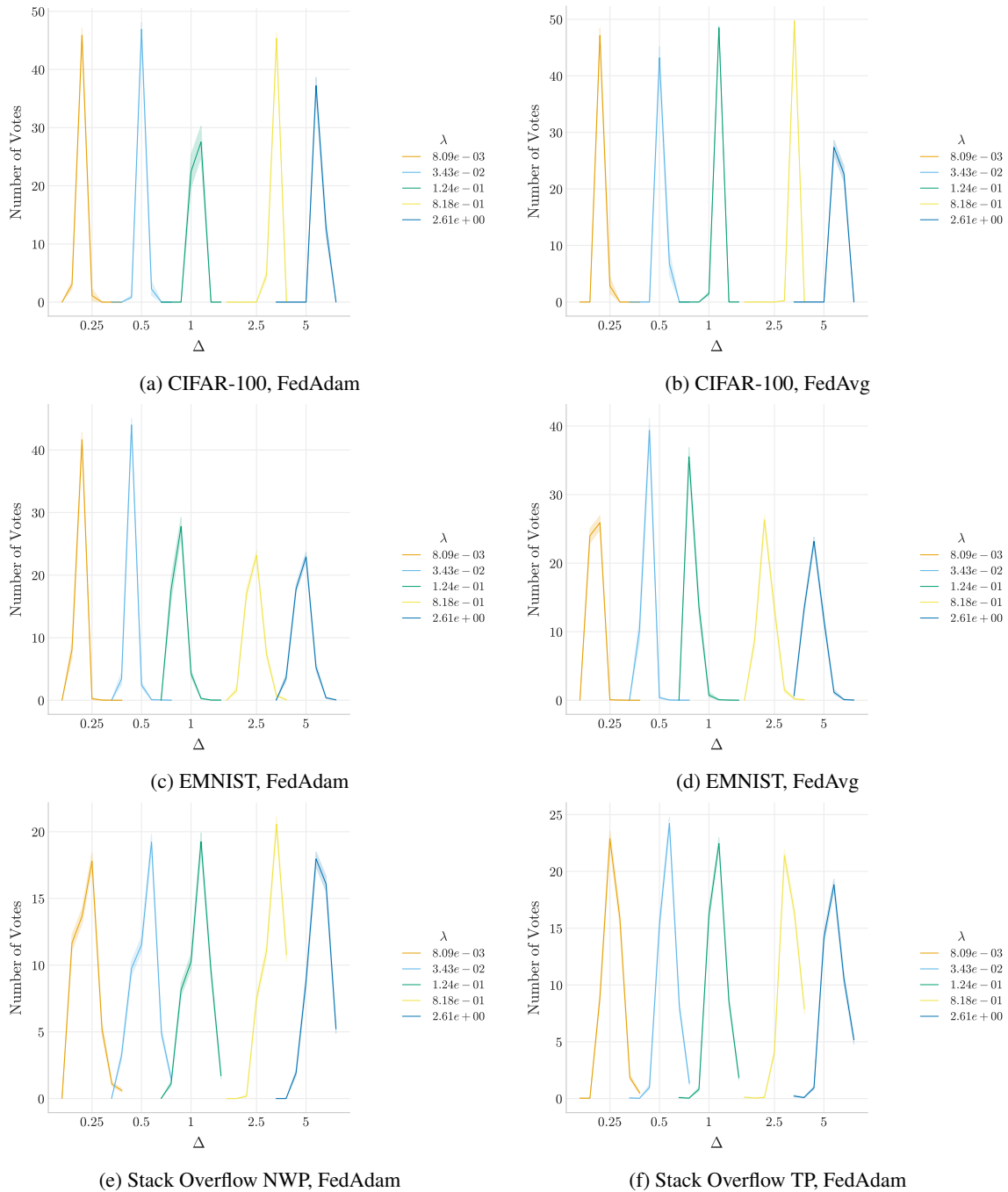


Figure 19. Histograms on selected  $\Delta$  for a given  $\lambda$ , averaged across training rounds.

**B.7. Overall Results**

The same experiment as in Figure 9, with other tasks and optimizers. Our method significantly outperforms Top-K, DRIVE, and 3LC. Performance is similar to QSGD on tasks with relatively similar data on clients (CIFAR-100 and EMNIST), with a visible gap in Stack Overflow tasks.

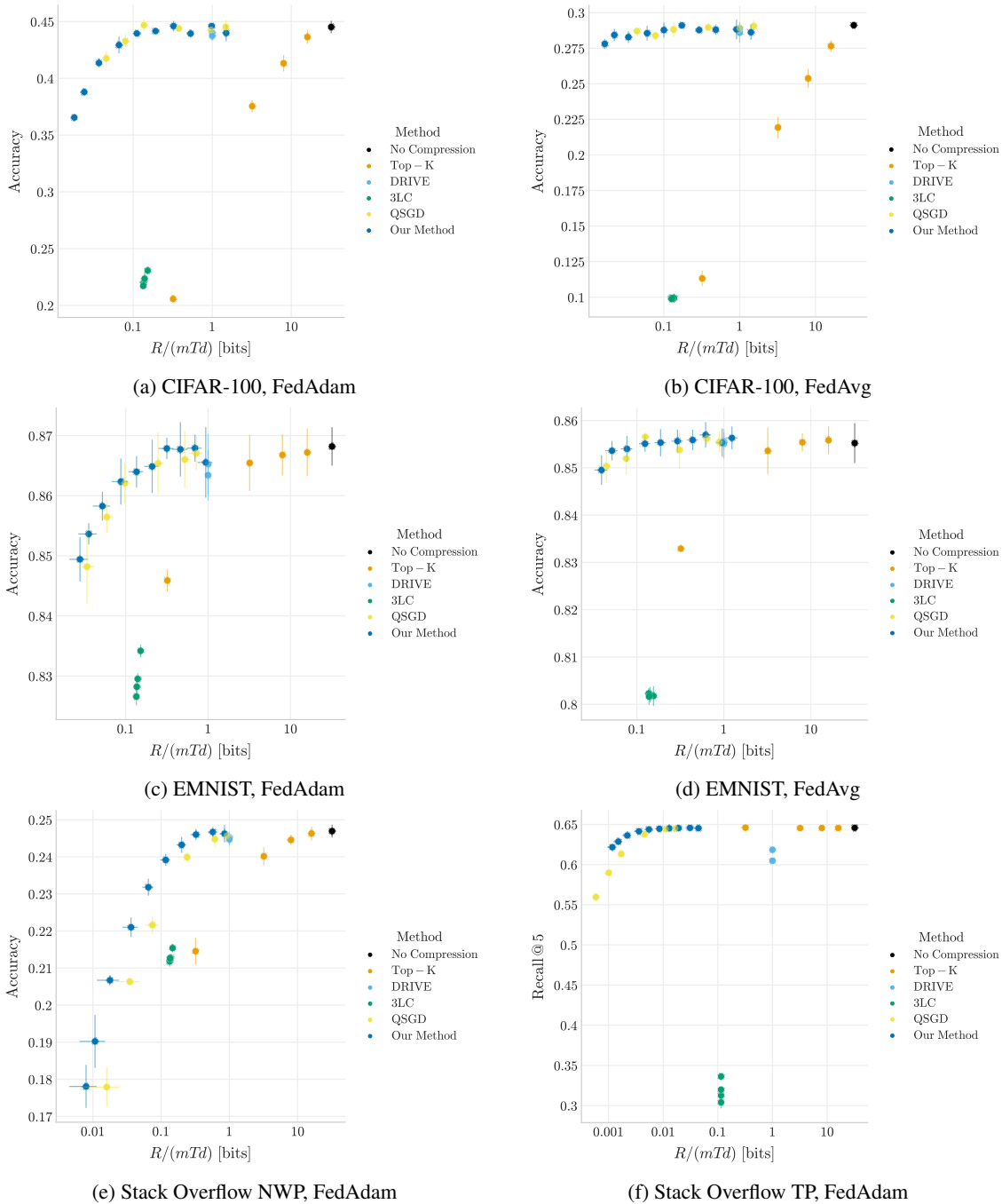


Figure 20. Our method performs competitively against all others in terms of the accuracy–communication cost trade-off. We use a range of  $\Delta \in \{0.05..17.5\}$ . Error bars indicate variance in average per-coordinate rate and final model accuracy over five random trials.

## B.8. Rotations

The same experiment as in Figure 10, with other tasks and optimizers. The rate–distortion tradeoff is significantly better without rotation for EMNIST and Stack Overflow datasets. It is only slightly better for CIFAR-100, due to the fact that the client updates are not as sparse as for the other tasks.

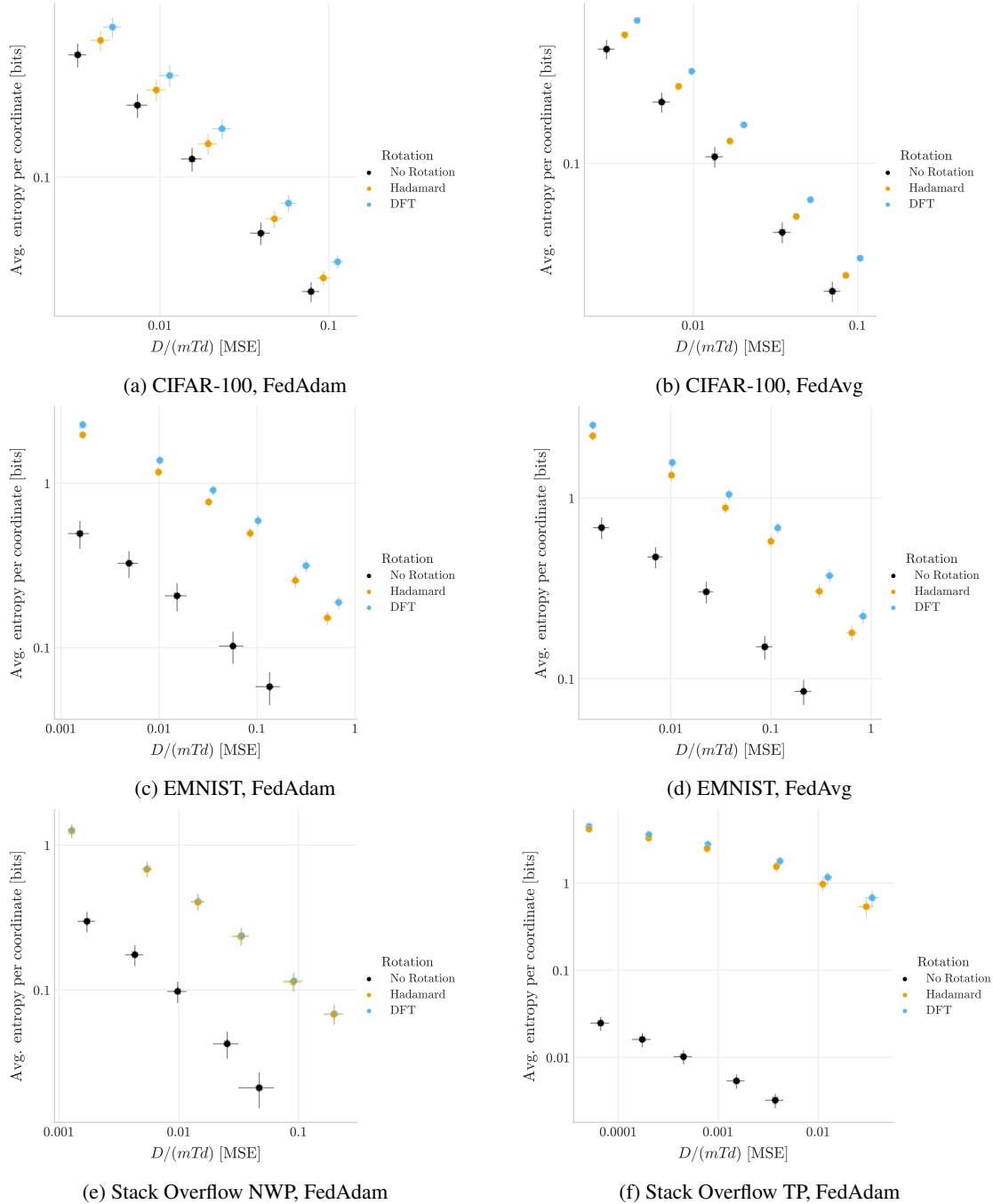


Figure 21. Transforming the client updates via a random rotation increases both entropy and distortion, producing a distribution with a worse entropy–distortion frontier. The effect is most dramatic on highly structured client updates. Error bars indicate variance in average per-coordinate distortion and average per-coordinate entropy over five random trials.

The same experiment as in Figure 11, across tasks and optimizers. Applying a fixed arbitrary rotation yields a lighter-tailed distribution with higher entropy. The effect is especially dramatic on the highly sparse client updates for the EMNIST and Stack Overflow tasks.

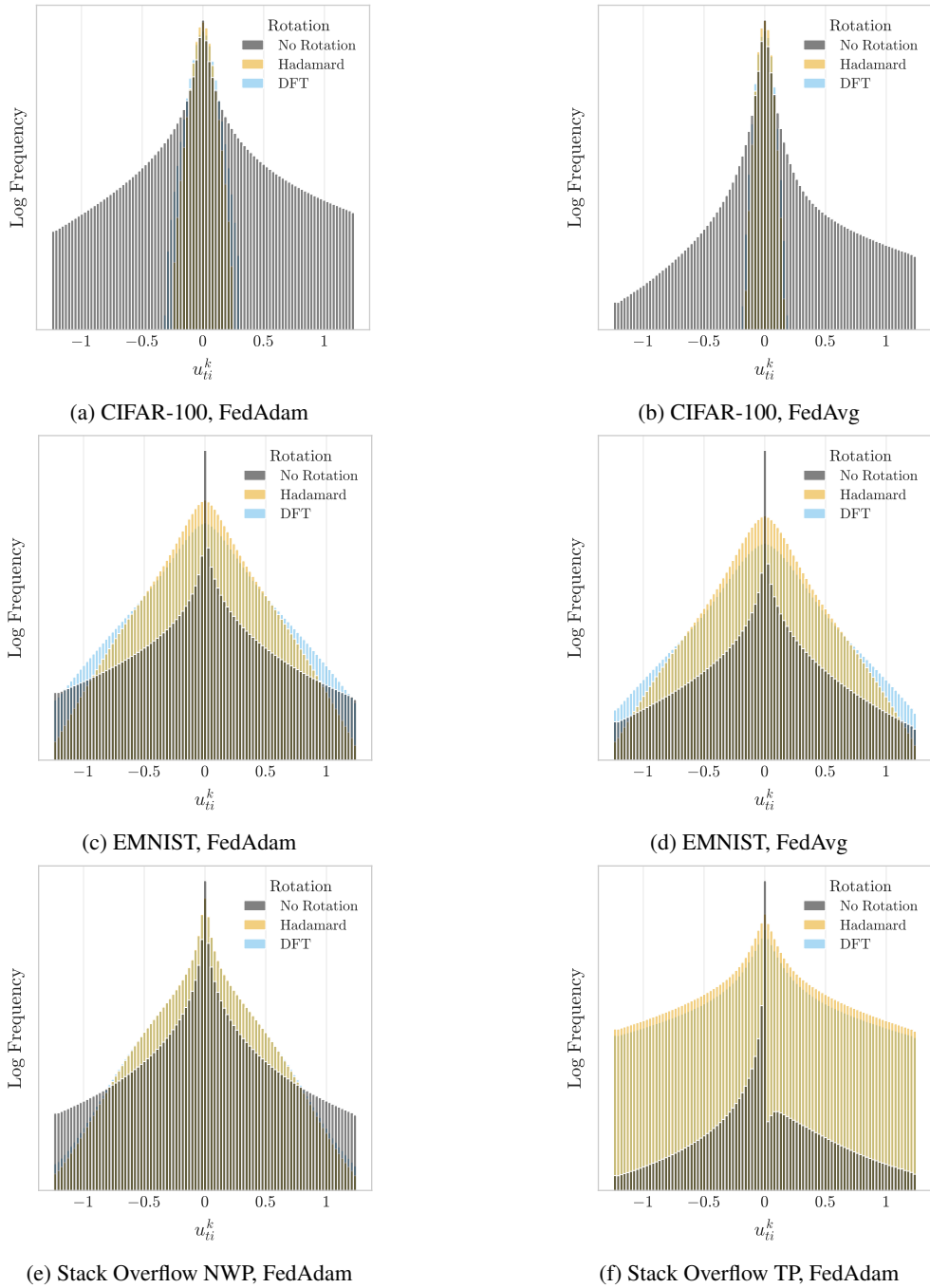


Figure 22. Transforming the client updates via a fixed rotation produces a lighter-tailed distribution with higher entropy. The effect is most dramatic on highly structured client updates.

### B.9. Normalization

The same experiment as in Figure 12, with other tasks and optimizers. QSGD yields similar performance on the CIFAR-100 dataset, where the clients have the same amount of training data. The gain in performance by our method is more pronounced on the more heterogeneous Stack Overflow tasks.

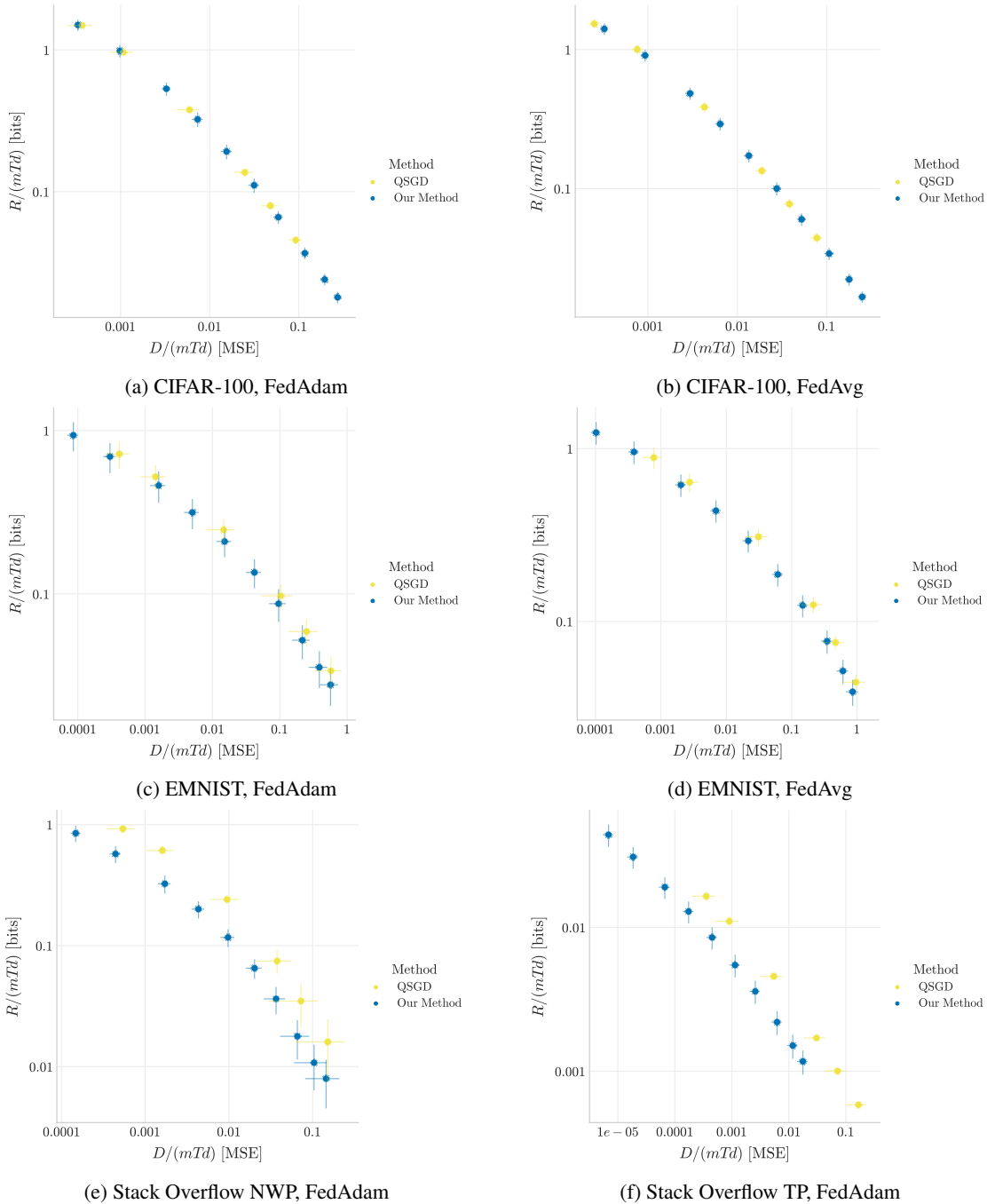


Figure 23. Transforming heterogeneous client updates via normalization results in a slightly worse rate–distortion performance. The effect is negligible on tasks with client updates of the same magnitude. Error bars indicate variance in average per-coordinate distortion and average per-coordinate rate over five random trials.

### B.10. Decaying $\Delta$

The same experiment as in Figure 13, with other tasks. We decay  $\Delta$  over the course of training according to an exponential decay schedule specified by  $\Delta_t = (\Delta_0 - \Delta_{min})e^{-\rho t} + \Delta_{min}$ . We select  $\rho$ , such that  $\Delta_T \approx \Delta_{min}$  for  $T = 1500$ . For the Stack Overflow next-word prediction task we set  $\Delta_0 = 10.0$ ,  $\Delta_{min} = 0.1$  and  $\rho = 0.006$ . For the other tasks we set  $\Delta_0 = 20.0$ ,  $\Delta_{min} = 1.0$  and  $\rho = 0.004$ . We observe that spending fewer bits initially and more bits later can improve the validation accuracy achieved for the cumulative communication cost incurred during training.

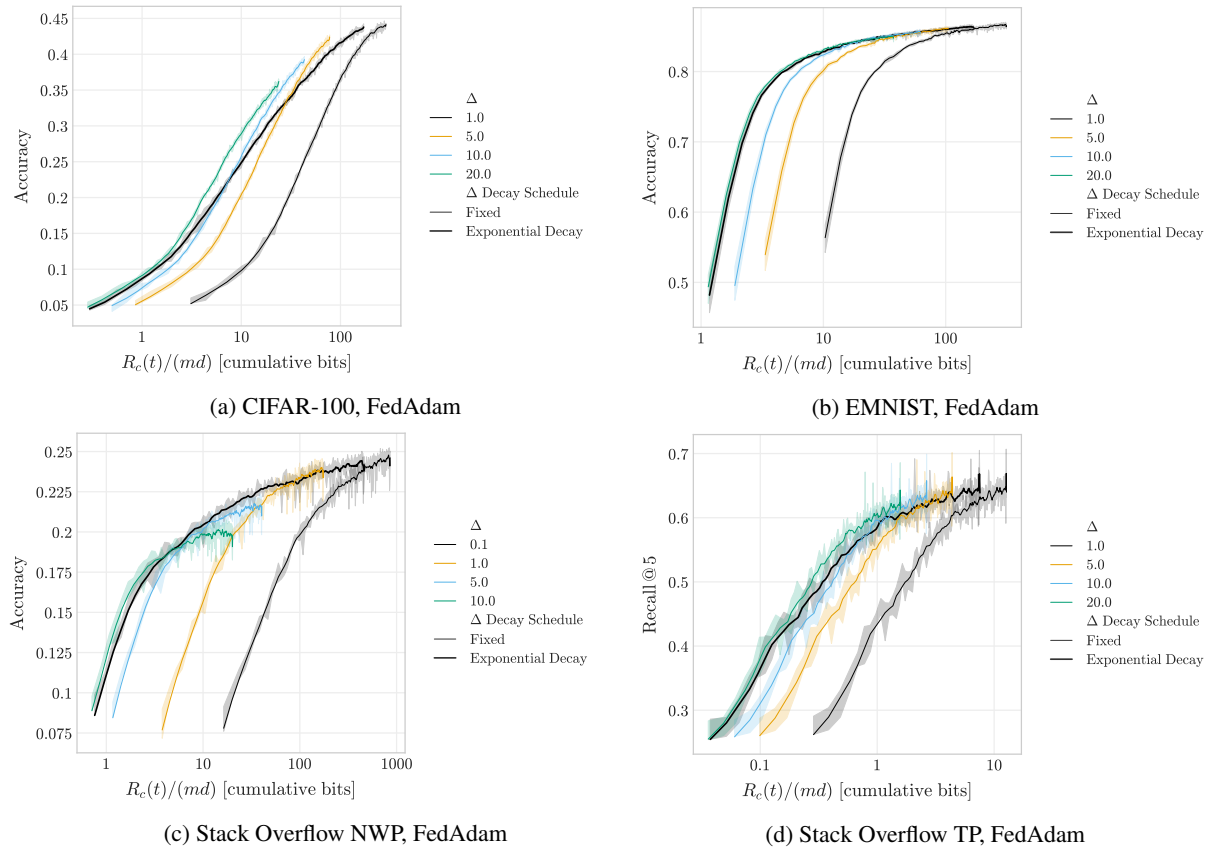


Figure 24. Exponentially decaying  $\Delta$  results in improved performance over keeping  $\Delta$  fixed when measuring the validation accuracy achieved for the cumulative bits spent on communicating each coordinate. This is particularly apparent on the Stack Overflow and EMNIST tasks. Here,  $\Delta$  is exponentially decayed from 10.0 to 0.1 on Stack Overflow NWP and from 20.0 to 1.0 on CIFAR-100, EMNIST and Stack Overflow TP, and compared to fixed  $\Delta$  within the respective decayed interval.